

# A series of energetic eruptions leading to a peculiar H-rich explosion of a massive star

Iair Arcavi<sup>1,2,3,4</sup>, D. Andrew Howell<sup>1,3</sup>, Daniel Kasen<sup>5,7,8</sup>, Lars Bildsten<sup>2,3</sup>, Griffin Hosseinzadeh<sup>1,3</sup>, Curtis McCully<sup>1,3</sup>, Zheng Chuen Wong<sup>1,3</sup>, Sarah Rebekah Katz<sup>1,3</sup>, Avishay Gal-Yam<sup>9</sup>, Jesper Sollerman<sup>10</sup>, Francesco Taddia<sup>10</sup>, Giorgos Leloudas<sup>9,11</sup>, Christoffer Fremling<sup>10</sup>, Peter E. Nugent<sup>6,8</sup>, Assaf Horesh<sup>12,9</sup>, Kunal Mooley<sup>13</sup>, Clare Rumsey<sup>14</sup>, S. Bradley Cenko<sup>15,16</sup>, Melissa L. Graham<sup>17,7,8</sup>, Daniel A. Perley<sup>11</sup>, Ehud Nakar<sup>18</sup>, Nir J. Shaviv<sup>12</sup>, Omer Bromberg<sup>18</sup>, Ken J. Shen<sup>7,8</sup>, Eran O. Ofek<sup>9</sup>, Yi Cao<sup>19</sup>, Xiaofeng Wang<sup>20</sup>, Fang Huang<sup>20</sup>, Liming Rui<sup>20</sup>, Tianmeng Zhang<sup>21</sup>, Wenxiong Li<sup>20</sup>, Zhitong Li<sup>20</sup>, Jujia Zhang<sup>22,23</sup>, Stefano Valenti<sup>24</sup>, David Guevel<sup>1,3</sup>, Benjamin Shappee<sup>25,26</sup>, Christopher S. Kochanek<sup>27,28</sup>, Thomas W.-S. Holoién<sup>27,28</sup>, Alexei V. Filippenko<sup>7,8</sup>, Rob Fender<sup>13</sup>, Anders Nyholm<sup>10</sup>, Ofer Yaron<sup>9</sup>, Mansi M. Kasliwal<sup>19</sup>, Mark Sullivan<sup>29</sup>, Nadja Blagorodnova<sup>19</sup>, Richard S. Walters<sup>19</sup>, Ragnhild Lunnan<sup>19</sup>, Danny Khazov<sup>9</sup>, Igor Andreoni<sup>30,31,32</sup>, Russ R. Laher<sup>33</sup>, Nick Konidaris<sup>34</sup>, Przemek Wozniak<sup>35</sup> and Brian Bue<sup>36</sup>

<sup>1</sup>*Las Cumbres Observatory, Goleta, CA 93117, USA*

<sup>2</sup>*Kavli Institute for Theoretical Physics, University of California, Santa Barbara, CA 93106, USA*

<sup>3</sup>*Department of Physics, University of California, Santa Barbara, CA 93106, USA*

<sup>4</sup>*Einstein Fellow*

<sup>5</sup>*Nuclear Science Division, Lawrence Berkeley National Laboratory, Berkeley, CA 94720, USA*

<sup>6</sup>*Computational Research Division, Lawrence Berkeley National Laboratory, Berkeley, CA 94720, USA*

<sup>7</sup>*Department of Physics, University of California, Berkeley, CA 94720, USA*

- <sup>8</sup>*Department of Astronomy, University of California, Berkeley, CA 94720-3411, USA*
- <sup>9</sup>*Department of Particle Physics and Astrophysics, The Weizmann Institute of Science, Rehovot, 76100, Israel*
- <sup>10</sup>*The Oskar Klein Centre, Department of Astronomy, Stockholm University, AlbaNova, SE-10691 Stockholm, Sweden*
- <sup>11</sup>*Dark Cosmology Centre, Niels Bohr Institute, University of Copenhagen, Juliane Maries vej 30, 2100 Copenhagen, Denmark*
- <sup>12</sup>*Racah Institute of Physics, The Hebrew University of Jerusalem, Jerusalem 91904, Israel*
- <sup>13</sup>*Department of Physics, Astrophysics, University of Oxford, Denys Wilkinson Building, Oxford, OX1 3RH, UK*
- <sup>14</sup>*Astrophysics Group, Cavendish Laboratory, 19 J. J. Thomson Avenue, Cambridge, CB3 0HE*
- <sup>15</sup>*Astrophysics Science Division, NASA Goddard Space Flight Center, Code 661, Greenbelt, MD 20771, USA*
- <sup>16</sup>*Joint Space-Science Institute, University of Maryland, College Park, MD 20742, USA*
- <sup>17</sup>*Department of Astronomy, University of Washington, Box 351580, U.W., Seattle, WA 98195-1580*
- <sup>18</sup>*The Raymond and Beverly Sackler School of Physics and Astronomy, Tel Aviv University, Tel Aviv 69978, Israel*
- <sup>19</sup>*Cahill Center for Astrophysics, California Institute of Technology, Pasadena, CA 91125, USA*
- <sup>20</sup>*Physics Department and Tsinghua Center for Astrophysics (THCA), Tsinghua University, Beijing, 100084, China*

<sup>21</sup>*National Astronomical Observatories of China, Chinese Academy of Sciences, Beijing, 100012, China*

<sup>22</sup>*Yunnan Observatories, Chinese Academy of Sciences, Kunming 650011, China*

<sup>23</sup>*Key Laboratory for the Structure and Evolution of Celestial Objects, Chinese Academy of Sciences*

<sup>24</sup>*Department of Physics, University of California, 1 Shields Ave, Davis, CA 95616, USA*

<sup>25</sup>*Carnegie Observatories, 813 Santa Barbara Street, Pasadena, CA 91101, USA*

<sup>26</sup>*Hubble Fellow, Carnegie-Princeton Fellow*

<sup>27</sup>*Department of Astronomy, The Ohio State University, 140 West 18th Avenue, Columbus, OH 43210, USA*

<sup>28</sup>*Center for Cosmology and AstroParticle Physics (CCAPP), The Ohio State University, 191 W. Woodruff Ave., Columbus, OH 43210, USA*

<sup>29</sup>*Department of Physics and Astronomy, University of Southampton, Southampton SO17 1BJ, UK*

<sup>30</sup>*Centre for Astrophysics and Supercomputing, Swinburne University of Technology, PO Box 218, VIC 3122, Australia*

<sup>31</sup>*ARC Centre of Excellence for All-sky Astrophysics (CAASTRO)*

<sup>32</sup>*Australian Astronomical Observatory, PO Box 915, North Ryde, NSW 1670, Australia*

<sup>33</sup>*Spitzer Science Center, California Institute of Technology, MS 314-6, Pasadena, CA 91125, USA*

<sup>34</sup>*Kairos Aerospace, 777 Cuesta Drive, Suite 202, Mountain View, CA, 94040*

<sup>35</sup>*Space and Atmospheric Sciences Group, Mail Stop D466, Los Alamos National Laboratory, Los*

*Alamos, NM 87545*

<sup>36</sup>*Jet Propulsion Laboratory, California Institute of Technology, Pasadena, CA 91109, USA*

1 **Every supernova hitherto observed has been the terminal explosion of a star. And all su-**  
2 **pernovae with absorption lines in their spectra show those lines decreasing in velocity over**  
3 **time, as the ejecta expands and thins, revealing slower moving material that was previously**  
4 **hidden. In addition, every supernova that shows absorption lines of hydrogen has one main**  
5 **lightcurve peak, or a plateau in luminosity for approximately 100 days before declining<sup>1</sup>.**  
6 **Here we report observations of iPTF14hls, an event that has spectra identical to a hydrogen-**  
7 **rich core-collapse supernova, but which violates all of the above supernova principles: The**  
8 **lightcurve has at least five peaks and stays bright for more than 600 days; The absorption**  
9 **lines show little to no decrease in velocity; The radius of the line-forming region is more than**  
10 **an order of magnitude bigger than the radius of the photosphere derived from the continuum**  
11 **emission. This is consistent with a shell of a few 10's of solar masses ejected by the star at**  
12 **supernova-level energies a few hundred days prior to a terminal explosion. Another possible**  
13 **eruption was recorded at the same position in 1954. Multiple energetic pre-supernova erup-**  
14 **tions are expected to occur in  $\approx 95\text{--}130$  solar mass stars which experience the pulsational pair**  
15 **instability<sup>2, 3, 4, 5</sup>. However, that scenario does not account for the continued presence of hy-**  
16 **drogen nor the energetics observed here, prompting the need for a new violent mass ejection**  
17 **mechanism for massive stars.**

18 On 2014 Sep. 22.53 (UT dates are used throughout), the iPTF survey<sup>6, 7</sup> discovered iPTF14hls  
19 at right ascension,  $\alpha_{J2000} = 09\text{h } 20\text{m } 34.30\text{s}$  and declination,  $\delta_{J2000} = +50^{\circ}41'46.8''$ , at an  $R$ -band  
20 magnitude of  $17.716 \pm 0.033$  (Extended Data Fig. 1). We have no observations of this position  
21 between 2014 May 28 and Sep 22, inducing a  $\approx 100$ -day uncertainty in the explosion time, so

22 we use the discovery date as a reference epoch for all phases. We adopt a redshift of  $z = 0.0344$ ,  
23 determined from narrow host-galaxy features, corresponding to a luminosity distance of 156 Mpc<sup>9</sup>.

24 On 2015 Jan. 8, iPTF14hls was classified as a Type II-P supernova based on prominent  
25 broad Balmer series P-Cygni lines in an optical spectrum<sup>8</sup>. So far, Type II-P supernovae have  
26 been the only events ever observed to produce such spectra. In a Type II-P, the core of a massive  
27 star collapses to create a neutron star, sending a shock through the outer hydrogen-rich envelope,  
28 ejecting it. The shock ionizes the ejecta, which later expand, cool and recombine. The photosphere  
29 follows the recombination front, which is at a roughly constant temperature ( $T \approx 6000$  K) as it  
30 makes its way inward in mass through the expanding ejecta<sup>10</sup>. This leads to the  $\approx 100$ -day “plateau”  
31 phase of roughly constant luminosity in the light curve and prominent hydrogen P-Cygni features  
32 in the spectrum.

33 iPTF14hls, while identical to Type II-P supernovae in its spectroscopic features, has sev-  
34 eral properties never before seen in a supernova. Instead of a 100-day plateau, the light curve  
35 of iPTF14hls lasts over 600 days and has at least five distinct peaks during which the luminosity  
36 varies by as much as  $\approx 50\%$  (Fig. 1). Blackbody fits to the broad-band optical *BVgi* photometry  
37 of iPTF14hls (see Methods) indicate a roughly constant effective temperature of 5000–6000 K, the  
38 same as the hydrogen-recombination temperature typically seen in Type II-P supernovae. However,  
39 the inferred bolometric luminosity of a few  $\times 10^{42}$  erg s<sup>-1</sup> is on the high end of typical Type II-P  
40 supernovae<sup>11</sup>, and the total radiated energy of  $2.20_{-0.05}^{+0.03} \times 10^{50}$  erg emitted during the 450 days of  
41 our multi-band optical coverage is a few times larger than that of any known Type II-P supernova.

42 Given the uncertainty in explosion time of iPTF14hls, the discrepancies with Type II-P supernova  
43 timescales and energetics may be even larger.

44 The spectroscopic evolution of iPTF14hls is even harder to understand. It is a factor of  $\approx 10$   
45 slower than that of Type II-P supernovae (Fig. 2); e.g. the spectrum of iPTF14hls at 600 days looks  
46 like a normal SN II-P at 60 days (Extended Data Fig. 4). In all previously observed supernovae,  
47 the faster material is outside — spectra show a decrease of all measured velocities with time (by  
48 a factor of  $\approx 3$  over 100 days) as the material expands, thins, and the photosphere moves inward  
49 in mass revealing deeper, slower-moving material. In iPTF14hls, velocities of hydrogen decline  
50 by only 25%, from  $8000 \text{ km s}^{-1}$  to  $6000 \text{ km s}^{-1}$  over 600 days, while iron lines stay at a constant  
51 velocity of  $4000 \text{ km s}^{-1}$  (Fig. 3).

52 It is normal to see hydrogen lines at higher velocity than iron lines due to optical depth  
53 effects. But in time, as the material expands and thins, hydrogen should be seen at lower velocity  
54 where the iron was previously seen (Extended Data Figure 7). If the ejecta is expanding in size  
55 by a factor of  $\approx 6$  from day 100 to day 600, in the absence of an additional energy source, an  
56 inward-moving photosphere scanning through the ejecta in velocity must occur.

57 An observation of constant velocity can thus be caused by: (1) a central-engine pushing  
58 material from the inside, sweeping the ejecta into a thin dense shell<sup>12, 13</sup>, or (2) the lines being far  
59 above the photosphere, detached from it. One dimensional central-engine models compress the  
60 iron and hydrogen lines to the same velocity, which is not the case for iPTF14hls (though multi-  
61 dimensional effects could alter this prediction). The line evolution can more readily be explained if

62 the lines are formed by ejecta from a prior eruption that happened a few years before the discovery  
63 of iPTF14hls and are detached from the continuum, which was formed in the terminal explosion  
64 (see Methods).

65 We estimate the position of the line-forming region as  $vt$ , where  $v$  is the observed expansion  
66 velocity of the material at time  $t$ . For Type II-P supernovae, this radius, when using the iron line  
67 velocities, is the same as the photospheric radius obtained by blackbody fits to the continuum  
68 emission, up to an order-unity “blackbody dilution factor”<sup>14, 15, 16</sup>. For iPTF14hls, the  $vt$ -inferred  
69 radius is instead larger than the blackbody-inferred radius by an order of magnitude on day 600  
70 (Fig. 4). The fact that the two radii are so different from each other indicates that the line-forming  
71 region in iPTF14hls is indeed spatially detached from the continuum-emitting photosphere, in  
72 contrast to what is observed in all known Type II-P supernovae.

73 The observations are thus consistent with the line-forming material being ejected in a massive  
74 and very energetic pre-supernova outburst, specifically in a shell on the order of a few tens of  
75 solar masses (see Methods). However, this requires a kinetic energy of  $\approx 10^{52}$  erg, normally  
76 associated with a supernova. Further evidence for a third even earlier explosion comes from an  
77  $M_R \approx -15.6$  magnitude outburst detected at the position of iPTF14hls in 1954 (formally a  $2.2\sigma$   
78 detection, though this is likely an underestimate due to photographic nonlinearity; see Methods).

79 Another question is what is powering the light curve of iPTF14hls. Strong asymmetry may  
80 induce a luminosity increase in a particular direction. However, we do not detect any significant po-  
81 larization which would be indicative of asymmetry in the explosion (see Methods). An additional



82 energy source in iPTF14hls compared to normal II-P events could come from the interaction of the  
83 ejecta with previously ejected shells. However, in cases of SNe interacting with dense circumstel-  
84 lar material, the interaction dominates the spectra in the form of a strong continuum together with  
85 broad, intermediate and narrow components of the Balmer series emission lines<sup>17, 18</sup>. None of these  
86 features are seen in the spectra of iPTF14hls (Fig. 2; Extended Data Fig. 5). We find no evidence  
87 of X-ray or radio emission (which are possible additional indicators of strong interaction)<sup>19</sup> in ob-  
88 servations taken during the brightest peak of the optical light curve (see Methods). It is possible  
89 any signs of interaction are being reprocessed by overlying, previously ejected material.

90         Either way, the progenitor of iPTF14hls likely experienced multiple energetic eruptions over  
91 the last decades of its life. Energetic eruptions are expected in stars with initial masses of  $\approx 95$ –  
92  $130 M_{\odot}$  (where  $M_{\odot}$  is the solar mass) which undergo an instability arising from the production  
93 of electron-positron pairs<sup>2</sup>. Interaction between the different shells and/or the supernova ejecta  
94 and the shells can produce a variety of luminous long-lived transients with highly structured light  
95 curves<sup>4, 5</sup> similar to that of iPTF14hls. Such pulsational-pair instability supernovae are expected  
96 to occur in low metallicity environments. iPTF14hls occurred in the outskirts of a low-mass star-  
97 forming galaxy, possibly of low metal content (see Methods).

98         However, models of stars undergoing the pulsational pair instability eject most of the hydro-  
99 gen envelope in the first eruption<sup>5</sup>, whereas for iPTF14hls a few tens of solar masses of hydrogen  
100 were retained in the envelope after the 1954 outburst. Another problem is that pulsational pair  
101 instability models can account for up to  $\sim 4 \times 10^{51}$  erg of kinetic energy in all eruptions together,

102 while  $\sim 10^{52}$  erg are required just for the most recent eruption that ejected the line-forming region  
103 of iPTF14hls (see Methods).

104 iPTF14hls demonstrates that stars in the local Universe can undergo very massive eruptions  
105 in the decades leading to their collapse yet, surprisingly, maintain a massive hydrogen-rich en-  
106 velope for most of this period. Current models of massive star evolution and explosion need to  
107 be modified, or a completely new picture needs to be put forward, to account for the energetics of  
108 iPTF14hls, the lack of strong interaction signatures and the inferred amount of hydrogen it retained  
109 towards the end of its life.

- 110 1. Arcavi, I. Hydrogen-Rich Core-Collapse Supernovae. In *Handbook of Supernovae*, 1–38  
112 (Springer International Publishing, Cham, 2016). URL [http://link.springer.com/  
113 10.1007/978-3-319-20794-0\\_{\\_}39-1](http://link.springer.com/10.1007/978-3-319-20794-0_{_}39-1).
- 114 2. Barkat, Z., Rakavy, G. & Sack, N. Dynamics of Supernova Explosion Resulting from Pair  
115 Formation. *Physical Review Letters* **18**, 379–381 (1967). URL [http://link.aps.org/  
116 doi/10.1103/PhysRevLett.18.379](http://link.aps.org/doi/10.1103/PhysRevLett.18.379).
- 117 3. Heger, A. & Woosley, S. E. The Nucleosynthetic Signature of Population III.  
118 *The Astrophysical Journal*, Volume 567, Issue 1, pp. 532-543. **567**, 532–543 (2002).  
119 URL <http://arxiv.org/abs/astro-ph/0107037>[http://dx.doi.org/10.  
120 1086/338487](http://dx.doi.org/10.1086/338487). 0107037.
- 121 4. Woosley, S. E., Blinnikov, S. & Heger, A. Pulsational pair instability as an explanation

- 122 for the most luminous supernovae. *Nature*, Volume 450, Issue 7168, pp. 390-392 (2007).  
123 **450**, 390–392 (2007). URL <http://arxiv.org/abs/0710.3314><http://dx.doi.org/10.1038/nature06333>. 0710.3314.  
124
- 125 5. Woosley, S. E. Pulsational Pair-instability Supernovae. *The Astrophysical Journal* **836**,  
126 244 (2017). URL [http://stacks.iop.org/0004-637X/836/i=2/a=244?key=](http://stacks.iop.org/0004-637X/836/i=2/a=244?key=crossref.26431d83a9818abda1d8363b62462c1e)  
127 [crossref.26431d83a9818abda1d8363b62462c1e](http://stacks.iop.org/0004-637X/836/i=2/a=244?key=crossref.26431d83a9818abda1d8363b62462c1e).
- 128 6. Law, N. M. *et al.* The Palomar Transient Factory: System Overview, Performance and  
129 First Results. *Publications of the Astronomical Society of the Pacific* **121**, 1395–1408  
130 (2009). URL <http://arxiv.org/abs/0906.5350>[http://dx.doi.org/10.](http://dx.doi.org/10.1086/648598)  
131 [1086/648598](http://dx.doi.org/10.1086/648598). 0906.5350.
- 132 7. Rau, A. *et al.* Exploring the Optical Transient Sky with the Palomar Transient Factory. *Publi-*  
133 *cations of the Astronomical Society of the Pacific* **121**, 1334–1351 (2009). URL [http://](http://arxiv.org/abs/0906.5355)  
134 [arxiv.org/abs/0906.5355](http://arxiv.org/abs/0906.5355)<http://dx.doi.org/10.1086/605911>. 0906.  
135 5355.
- 136 8. Li, W., Wang, X. & Zhang, T. Spectroscopic Classification of CSS141118:092034+504148 as  
137 a Type II-P Supernova. *The Astronomer's Telegram* **6898** (2015).
- 138 9. Planck Collaboration *et al.* Planck 2015 results. XIII. Cosmological parameters (2015).  
139 1502.01589.

- 140 10. Popov, D. V. An analytical model for the plateau stage of Type II supernovae. *The Astrophys-*  
141 *ical Journal* **414**, 712 (1993). URL [http://adsabs.harvard.edu/doi/10.1086/](http://adsabs.harvard.edu/doi/10.1086/173117)  
142 173117.
- 143 11. Bersten, M. C. & Hamuy, M. Bolometric Light Curves For 33 Type II Plateau Supernovae.  
144 *The Astrophysical Journal* **701**, 200–208 (2009). URL [http://adsabs.harvard.edu/](http://adsabs.harvard.edu/abs/2009ApJ...701..200B)  
145 [abs/2009ApJ...701..200B](http://adsabs.harvard.edu/abs/2009ApJ...701..200B).
- 146 12. Kasen, D. & Bildsten, L. Supernova Light Curves Powered by Young Magnetars. *The As-*  
147 *trophysical Journal* **717**, 245–249 (2010). URL [http://adsabs.harvard.edu/abs/](http://adsabs.harvard.edu/abs/2010ApJ...717..245K)  
148 [2010ApJ...717..245K](http://adsabs.harvard.edu/abs/2010ApJ...717..245K).
- 149 13. Dexter, J. & Kasen, D. Supernova Light Cuves Powered by Fallback Accretion. *The Astro-*  
150 *physical Journal* **772**, 30 (2013). URL [http://stacks.iop.org/0004-637X/772/](http://stacks.iop.org/0004-637X/772/i=1/a=30?key=crossref.6ebc8a4f6831234f803ea155f05e61e2)  
151 [i=1/a=30?key=crossref.6ebc8a4f6831234f803ea155f05e61e2](http://stacks.iop.org/0004-637X/772/i=1/a=30?key=crossref.6ebc8a4f6831234f803ea155f05e61e2).
- 152 14. Kirshner, R. P. & Kwan, J. The envelopes of type II supernovae. *The Astrophysical Jour-*  
153 *nal* **197**, 415 (1975). URL [http://adsabs.harvard.edu/abs/1975ApJ...197.](http://adsabs.harvard.edu/abs/1975ApJ...197..415K)  
154 [.415K](http://adsabs.harvard.edu/abs/1975ApJ...197..415K).
- 155 15. Eastman, R. G., Schmidt, B. P. & Kirshner, R. The Atmospheres of Type II Supernovae  
156 and the Expanding Photosphere Method. *The Astrophysical Journal* **466**, 911 (1996). URL  
157 <http://adsabs.harvard.edu/doi/10.1086/177563>.

- 158 16. Dessart, L. & Hillier, D. J. Distance determinations using type II supernovae and the expanding  
159 photosphere method. *Astronomy and Astrophysics* **439**, 671–685 (2005). URL [http://](http://www.edpsciences.org/10.1051/0004-6361:20053217)  
160 [www.edpsciences.org/10.1051/0004-6361:20053217](http://www.edpsciences.org/10.1051/0004-6361:20053217).
- 161 17. Schlegel, . A new subclass of Type II supernovae? *Monthly Notices of the Royal Astronomical*  
162 *Society (ISSN 0035-8711)* **244**, 269–271 (1990). URL [http://adsabs.harvard.edu/](http://adsabs.harvard.edu/abs/1990MNRAS.244..269S)  
163 [abs/1990MNRAS.244..269S](http://adsabs.harvard.edu/abs/1990MNRAS.244..269S).
- 164 18. Kiewe, M. *et al.* Caltech Core-Collapse Project (CCCP) Observations of Type II In Super-  
165 novae: Typical Properties and Implications for Their Progenitor Stars. *The Astrophysical Jour-*  
166 *nal* **744**, 10 (2012). URL [http://adsabs.harvard.edu/abs/2012ApJ...744.](http://adsabs.harvard.edu/abs/2012ApJ...744..10K)  
167 [..10K](http://adsabs.harvard.edu/abs/2012ApJ...744..10K).
- 168 19. Chevalier, R. A., Fransson, C. & Nymark, T. K. Radio and X-Ray Emission as Probes of Type  
169 IIP Supernovae and Red Supergiant Mass Loss. *The Astrophysical Journal, Volume 641, Issue*  
170 *2, pp. 1029-1038.* **641**, 1029–1038 (2006). URL [http://arxiv.org/abs/astro-ph/](http://arxiv.org/abs/astro-ph/0509468)  
171 [0509468](http://arxiv.org/abs/astro-ph/0509468)<http://dx.doi.org/10.1086/500528>. 0509468.
- 172 20. Geha, M. *et al.* Variability-Selected Quasars in MACHO Project Magellanic Cloud  
173 Fields. *The Astronomical Journal, Volume 125, Issue 1, pp. 1-12.* **125**, 1–12 (2003).  
174 URL <http://arxiv.org/abs/astro-ph/0209513>[http://dx.doi.org/10.](http://dx.doi.org/10.1086/344947)  
175 [1086/344947.0209513](http://arxiv.org/abs/astro-ph/0209513).
- 176 21. Michel, F. C. Neutron star disk formation from supernova fall-back and possible observa-  
177 tional consequences. *Nature* **333**, 644–645 (1988). URL <http://www.nature.com/>

178      doifinder/10.1038/333644a0.

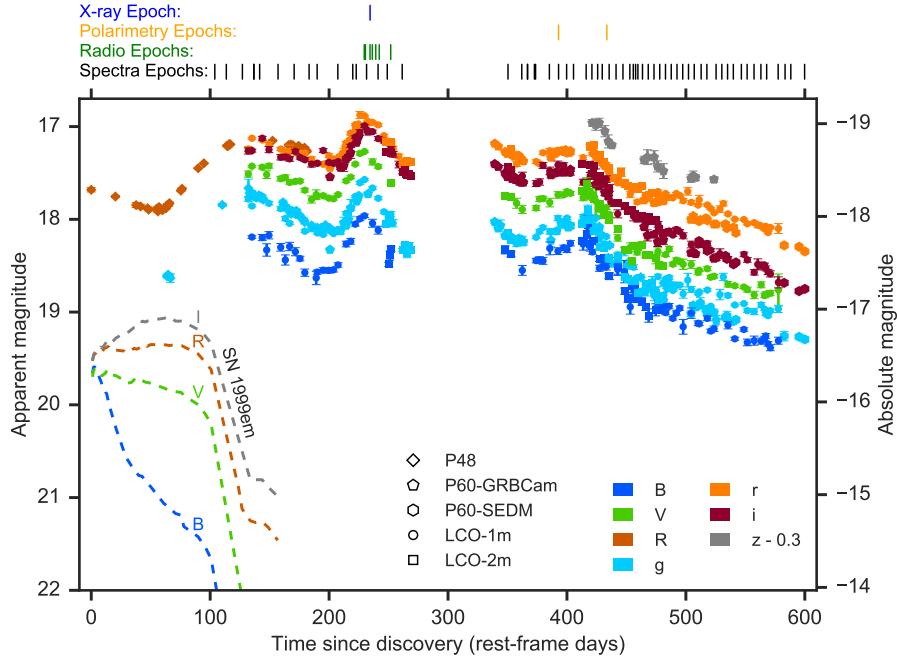
179 22. Leonard, D. *et al.* The Distance to SN 1999em in NGC 1637 from the Expanding Photosphere  
180 Method. *Publications of the Astronomical Society of the Pacific* **114**, 35–64 (2002). URL  
181 <http://adsabs.harvard.edu/abs/2002PASP...114...35L>.

182 **Competing Interests** The authors declare that they have no competing financial interests.

183 **Author Contributions** I. Arcavi initiated the study, triggered follow-up observations, reduced data, per-  
184 formed the analysis and wrote the manuscript. DAH is PI of the LCO Supernova Key Project through which  
185 all of the LCO data were obtained and assisted with interpretations, and the manuscript. DK and LB assisted  
186 with theoretical models, data interpretation and with the manuscript. GH and CM assisted with obtaining  
187 and reducing LCO data. ZCW first flagged the supernova as interesting. SRK performed the spectral ex-  
188 pansion velocity measurements. AGY is the PI for core-collapse supernovae in iPTF and assisted with  
189 interpretations. JS and FT obtained the NOT spectra and polarimetry data and assisted with the manuscript.  
190 GL reduced the polarimetry data. CF reduced the P60 data. PEN discovered the 1954 eruption image of  
191 iPTF14hls, helped obtain the host-galaxy spectrum, and is a Co-PI on the Keck proposal under which it  
192 and one of the supernova spectra were obtained. AH obtained and reduced the VLA data and is PI of the  
193 program through which the data were obtained. KM and CR obtained and reduced the AMI data. SBC ob-  
194 tained and reduced the XRT data. MLG obtained and reduced Keck spectra. DAP performed the host-galaxy  
195 analysis and assisted with the manuscript. EN, OB, NJS and KJS assisted with theoretical interpretations  
196 and with the manuscript. EOO helped with interpretations and the manuscript. YC built the real-time iPTF  
197 image-subtraction pipeline and obtained P200 observations. XW, FH, LR, TZ, WL, ZL, and JZ obtained and  
198 reduced the Xinglong, Lijiang and TNT data. SV built the LCO photometric and spectroscopic reduction

199 pipelines and assisted with LCO observations, interpretation and the manuscript. DG assisted with the POSS  
200 image analysis. BS, CSK, and TW-SH obtained and reduced the ASAS-SN pre-discovery limits. AVF is a  
201 Co-PI of the Keck proposal under which the host-galaxy spectrum and one of the supernova spectra were  
202 obtained; he also helped with the manuscript. RF is PI of the program through which the AMI data were  
203 obtained. AN helped scan for iPTF candidates and assisted with the manuscript. OY is in charge of the iPTF  
204 candidate scanning effort. MMK lead the work for building iPTF. MS wrote the pipeline used to reduce P48  
205 data. NB and RSW obtained P60 SEDM photometry. RN, DK, and I. Andreoni obtained P200 observations.  
206 RRL contributed to building the P48 image-processing pipeline. NK was a main builder of the P60 SEDM.  
207 PW and BB helped build the machine learning algorithms that identify iPTF supernova candidates.

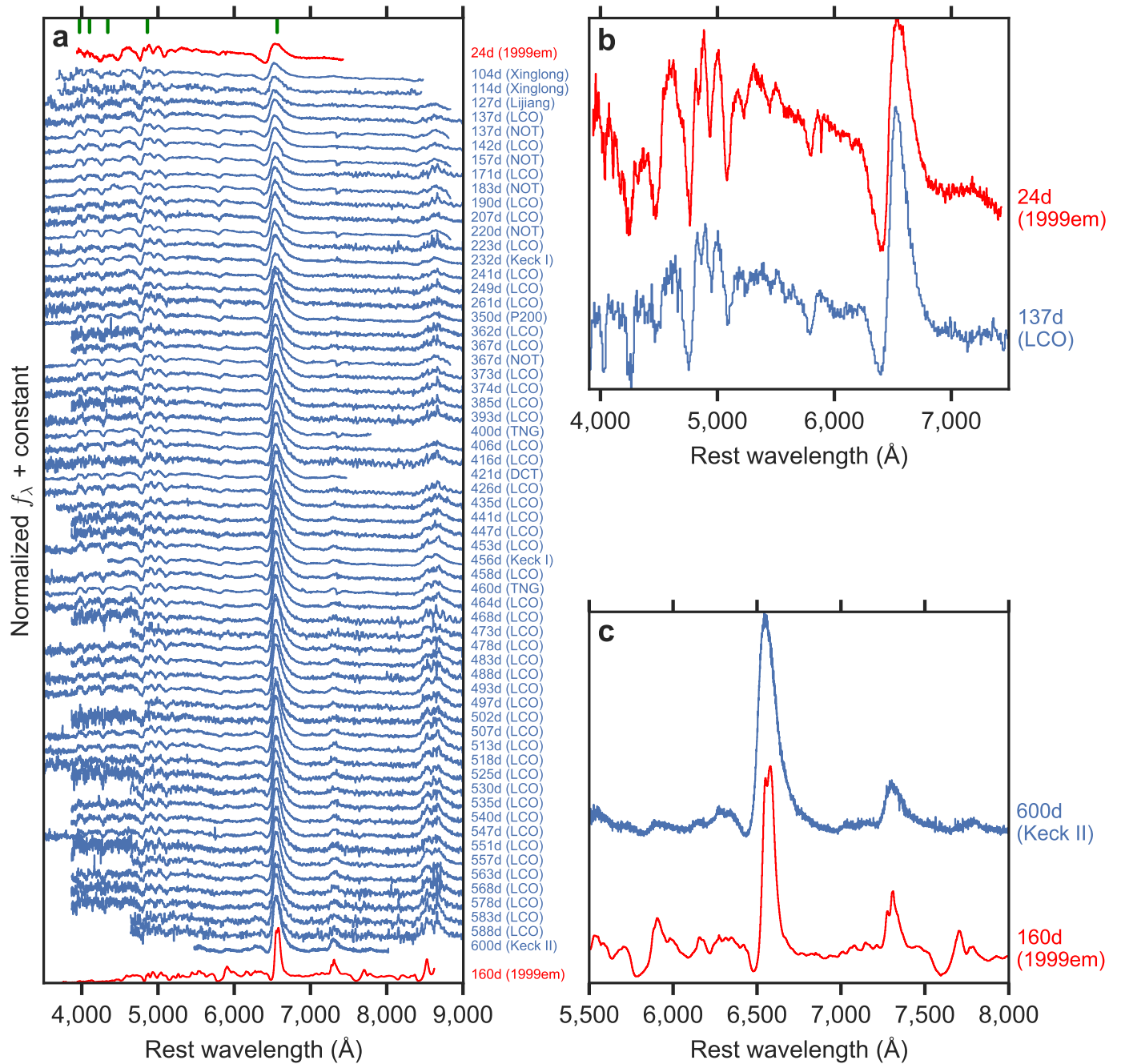
208 **Correspondence** Correspondence and requests for materials should be addressed to Iair Arcavi (email:  
209 arcavi@gmail.com).



210

211 **Figure 1** Multi-band optical light curves of iPTF14hls (overlapping data from additional  
 212 telescopes, not plotted here for clarity, are presented in Extended Data Fig. 2; see Meth-  
 213 ods for a list of participating telescopes). The prototypical Type II-P SN 1999em is shown  
 214 for comparison (dashed lines)<sup>22</sup>, according to the ordinate axis at right. Photometric points  
 215 from the same day, instrument, and filter are averaged for clarity. The SEDM *i*-band data  
 216 are shifted by +0.3 mag to compensate for filter differences with the other instruments.  
 217 iPTF14hls has at least five distinct peaks in its light curve (at approximately 140, 220,  
 218 and 410 days after discovery, before discovery as indicated by the *R*-band light curve,  
 219 and while the supernova was behind the Sun between days 260 and 340 after discovery).  
 220 Error bars denote  $1\sigma$  uncertainties.



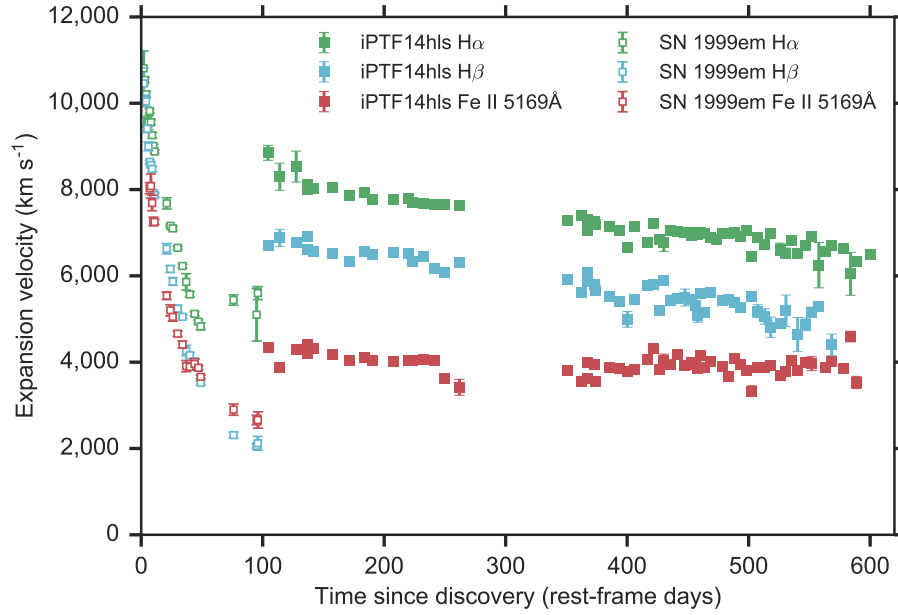


221

222

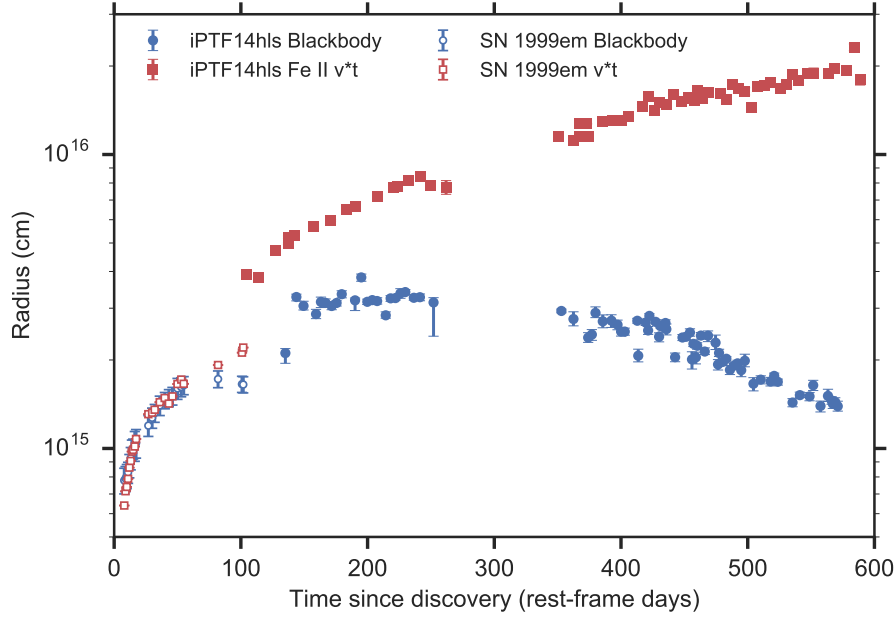
223 **Figure 2** Our full sequence (a) of optical spectra of iPTF14hls (blue) with select early-  
 224 time (b) and late-time (c) spectra blown up, expressed in terms of normalized flux density

225 as a function of rest-frame wavelength. The spectra are binned in wavelength and shifted  
226 in flux density for clarity. Phases are noted in rest-frame days since discovery on the  
227 ordinate axis at right, with the telescope used to obtain the spectrum in parentheses  
228 (see Methods for details). Spectra of the prototypical Type II-P SN 1999em<sup>22</sup> (red) are  
229 shown for comparison with phases noted in rest-frame days since explosion. Balmer se-  
230 ries hydrogen-line wavelengths are denoted in green tick marks at the top of panel (a).  
231 iPTF14hls is very similar spectroscopically to a normal Type II-P supernova but evolves  
232 much more slowly, beginning to become nebular only several hundred days after explo-  
233 sion, yet still showing continuum emission and high velocities even at day 600 (b). The  
234 spectral evolution is very smooth (a), in contrast to the multi-peaked light curve.



235

236 **Figure 3** Expansion velocities as a function of time, measured from the P-Cygni ab-  
 237 sorption features of three different spectral lines (see Methods) for iPTF14hls (filled sym-  
 238 bols) and the prototypical Type II-P SN 1999em<sup>22</sup> (empty symbols). Error bars denote  $1\sigma$   
 239 uncertainties and are sometimes smaller than the marker size. The velocities seen for  
 240 iPTF14hls evolve much more slowly compared to SN 1999em.



241

242 **Figure 4** The photospheric radius of iPTF14hls (filled symbols) estimated in two dif-  
 243 ferent ways: (1) Using blackbody fits to the broad-band  $BVgi$  photometry (blue) and (2)  
 244 using the derived expansion velocities of Fe II  $5169 \text{ \AA}$  (Fig. 3) times the elapsed rest-  
 245 frame time since discovery (red). The same quantities are shown for the prototypical  
 246 Type II-P SN 1999em (empty symbols; after correcting for the blackbody dilution factor)<sup>22</sup>.  
 247 Error bars denote  $1\sigma$  uncertainties and are sometimes smaller than the marker size. For  
 248 SN 1999em the radii overlap as expected, but for iPTF14hls they diverge, indicating that  
 249 the line-forming region may be detached from the photosphere (if the explosion occurred  
 250 before discovery the divergence is even more extreme).

251 **Supplementary Information**

252 We are grateful to C. Harris, D. Leonard, D. Poznanski, N. Smith and S. Woosley for comments  
253 and discussion, and to T. Pursimo for assistance with the polarimetry measurements.

254 Support for I. Arcavi was provided by NASA through the Einstein Fellowship Program, grant  
255 PF6-170148. This research is funded in part by the Gordon and Betty Moore Foundation through  
256 Grant GBMF5076 to LB and DK and by the National Science Foundation under grant PHY 11-  
257 25915. DAH, GH, and CM are supported by NSF grant AST-1313484. AGY is supported by the  
258 EU via ERC grants No. 307260 and 725161, the Quantum Universe I-Core program by the Israeli  
259 Committee for Planning and Budgeting, and the ISF; a Binational Science Foundation "Transfor-  
260 mative Science" grant and by a Kimmel award. JS gratefully acknowledges support from the Knut  
261 and Alice Wallenberg Foundation. KM acknowledges funding from the Hintze Trust. XW, TZ, and  
262 JZ are supported by Major State Basic Research Development Program (2013CB834903), the Na-  
263 tional Natural Science Foundation of China (NSFC grants: 11325313, 11403096 and 11633002),  
264 and the Strategic Priority Research Program of Emergence of Cosmological Structures of the Chi-  
265 nese Academy of Sciences (grant No. XDB09000000). AVF's supernova group at U.C. Berke-  
266 ley is supported by Gary & Cynthia Bengier, the Christopher R. Redlich Fund, the TABASGO  
267 Foundation, and NSF grant AST-1211916. Research support to I. Andreoni is provided by the  
268 Australian Astronomical Observatory (AAO). BS is supported by NASA through Hubble Fellow-  
269 ship grant HF-51348.001 awarded by the Space Telescope Science Institute, which is operated by  
270 the Association of Universities for Research in Astronomy, Inc., for NASA, under contract NAS  
271 5-26555. TW-SH is supported by the DOE Computational Science Graduate Fellowship, grant

272 number DEFG02-97ER25308. MS acknowledges support from EU/FP7-ERC grant 615929.

273       The Intermediate Palomar Transient Factory project is a scientific collaboration among the  
274 California Institute of Technology, Los Alamos National Laboratory, the University of Wisconsin,  
275 Milwaukee, the Oskar Klein Center, the Weizmann Institute of Science, the TANGO Program of  
276 the University System of Taiwan, and the Kavli Institute for the Physics and Mathematics of the  
277 Universe. LANL participation in iPTF was funded by the US Department of Energy as part of  
278 the Laboratory Directed Research and Development program. Part of this research was carried  
279 out at the Jet Propulsion Laboratory, California Institute of Technology, under a contract with the  
280 National Aeronautics and Space Administration. This paper made use of data from Las Cumbres  
281 Observatory global network of telescopes; the W. M. Keck Observatory, which is operated as a sci-  
282 entific partnership among the California Institute of Technology, the University of California, and  
283 NASA; the observatory was made possible by the generous financial support of the W. M. Keck  
284 Foundation; the Nordic Optical Telescope, operated by the Nordic Optical Telescope Scientific  
285 Association at the Observatorio del Roque de los Muchachos, La Palma, Spain, of the Instituto  
286 de Astrofísica de Canarias; ALFOSC, which is provided by the Instituto de Astrofísica de An-  
287 dalucía (IAA) under a joint agreement with the University of Copenhagen and NOTSA; DOLoRes  
288 on TNG; the Discovery Channel Telescope (DCT) at Lowell Observatory. Lowell is a private,  
289 nonprofit institution dedicated to astrophysical research and public appreciation of astronomy and  
290 operates the DCT in partnership with Boston University, the University of Maryland, the University  
291 of Toledo, Northern Arizona University and Yale University. The upgrade of the DeVeny optical  
292 spectrograph has been funded by a generous grant from John and Ginger Giovale. We thank the

293 support of the staffs at *Swift*, AMI-LA and the Xinglong Observatory (part of the National Astro-  
294 nomical Observatories of China) and the Lijiang Observatory (part of the Yunnan Observatories  
295 of China) for assistance with the observations. The AMI is supported by the European Research  
296 Council. Development of ASAS-SN has been supported by NSF grant AST-0908816 and CCAPP  
297 at the Ohio State University. ASAS-SN is supported by NSF grant AST-1515927, the Center for  
298 Cosmology and AstroParticle Physics (CCAPP) at OSU, the Mt. Cuba Astronomical Foundation,  
299 George Skestos, and the Robert Martin Ayers Sciences Fund. ASAS-SN thanks LCO and its staff  
300 for their continued support. The Digitized Sky Surveys were produced at the Space Telescope  
301 Science Institute under U.S. Government grant NAG W-2166. The National Geographic Society  
302 - Palomar Observatory Sky Atlas (POSS-I) was made by the California Institute of Technology  
303 with grants from the National Geographic Society. The Second Palomar Observatory Sky Sur-  
304 vey (POSS-II) was made by the California Institute of Technology with funds from the National  
305 Science Foundation, the National Geographic Society, the Sloan Foundation, the Samuel Oschin  
306 Foundation, and the Eastman Kodak Corporation.

307 **Methods**

308 **Discovery** The intermediate Palomar Transient Factory (iPTF) first detected iPTF14hls on 2014  
309 Sep 22.53 (Extended Data Fig. 1) using the iPTF real-time image-subtraction pipeline<sup>23</sup>. No source  
310 was seen at that position when it was previously visited by iPTF and by the All Sky Automated  
311 Survey for Supernova (ASAS-SN)<sup>24</sup> on 2014 May 6.19 and 2014 May 20-28 down to  $3\sigma$  limiting  
312 magnitudes of  $R < 20.95$  and  $V < 18.7$ , respectively. The source was observed by iPTF again  
313 on 2014 Oct. 13, Oct. 31, Nov. 4, and Nov. 10 before being saved and given a name as part  
314 of routine iPTF transient scanning. On 2014 Nov. 18, iPTF14hls was independently discovered  
315 by the Catalina Real-Time Transient Survey<sup>25</sup> as CSS141118:092034+504148, and later the event  
316 was reported to the Transient Name Server as AT 2016bse and Gaia16aog. On 2015 Feb. 3, upon  
317 routine LCO rescanning of previously saved iPTF candidates, we noticed the peculiar decline and  
318 subsequent rise of the light curve, and began an extensive campaign of spectroscopic and multi-  
319 band photometric follow-up observations.

320 **Followup Imaging** Followup imaging was obtained with the Palomar 48-inch Oschin Schmidt  
321 telescope (P48), the Palomar 60-inch telescope (P60)<sup>26</sup> using both the GRBCam and the SED  
322 Machine (SEDM) instruments, the Las Cumbres Observatory (LCO)<sup>27</sup> network 1-m and 2-m tele-  
323 scopes, and the 0.8-m Tsinghua University-NAOC telescope (TNT)<sup>28</sup> at the Xinglong Observa-  
324 tory. The TNT photometry is presented (together with CSS and Gaia photometry downloaded  
325 from their respective websites) in Extended Data Figure 2. P48 images were first pre-processed  
326 by the Infrared Processing and Analysis Center (IPAC)<sup>29</sup>. Image subtraction and point-spread-  
327 function (PSF) fitting was then performed<sup>30</sup> using pre-explosion images as templates. Magni-



328 tudes were calibrated to observations of the same field by the Sloan Digital Sky Survey (SDSS)  
329 DR10<sup>31</sup>. P60 images were pre-processed using a PyRAF-based pipeline<sup>26</sup>. Image subtraction,  
330 photometry extraction and calibration were performed with the `FPipe` pipeline<sup>32</sup> using SDSS  
331 images as references. LCO images were pre-processed using the Observatory Reduction and Ac-  
332 quisition Control Data Reduction pipeline (ORAC-DR)<sup>33</sup> up to 2016 May 4, and using the custom  
333 Python-based `BANZAI` pipeline afterward. Photometry was then extracted using the PyRAF-based  
334 `LCOsupernovapipeline` pipeline<sup>34</sup> to perform PSF fitting and calibration to the AAVSO Photomet-  
335 ric All-Sky Survey<sup>35</sup> for *BV*-band data and SDSS DR8<sup>36</sup> for *gri*-band data. TNT images were  
336 reduced with standard IRAF routines; PSF fitting was performed using the `SNOOPY` package and  
337 calibrated to the SDSS DR9<sup>37</sup> transformed to the Johnson system<sup>38</sup>. We correct all photometry  
338 for Milky Way extinction<sup>39</sup> extracted via the NASA Extragalactic Database (NED). Pre-explosion  
339 nondetection limits are presented in Extended Data Figure 3.

340 We fit a blackbody spectral energy distribution (SED) to every epoch of LCO photometry con-  
341 taining at least three of the *BVgi* filters obtained within 0.4 days of each other (we exclude *r* and  
342 *R*-band data from the fits owing to contamination from the  $H\alpha$  line). For each epoch we per-  
343 form a blackbody fit using Markov Chain Monte Carlo simulations through the Python `emcee`  
344 package<sup>40</sup> to estimate the blackbody temperature and radius at the measured distance to iPTF14hls  
345 of 156 Mpc.

346 **Followup Spectroscopy** Spectra of iPTF14hls were obtained with the Floyds instrument mounted  
347 on the northern LCO 2-m telescope<sup>27</sup>, the Andalucia Faint Object Spectrograph and Camera (AL-  
348 FOSC) mounted on the 2.5-m Nordic Optical Telescope (NOT), the Device Optimized for the LOW

349 RESolution (DOLoRes) mounted on the 3.6-m Telescopio Nazionale Galileo (TNG), the Low Res-  
350 olution Imaging Spectrometer (LRIS)<sup>41</sup> mounted on the Keck I 10-m telescope, the DEep Imaging  
351 Multi-Object Spectrograph (DEIMOS)<sup>42</sup> mounted on the Keck II 10-m telescope, the Double Beam  
352 Spectrograph (DBSP)<sup>43</sup> mounted on the Palomar 200-inch telescope (P200), the Beijing Faint Ob-  
353 ject Spectrograph and Camera (BFOSC) on the Xinglong 2.16-m telescope of the National Astro-  
354 nomical Observatories of China, the Yunnan Faint Object Spectrograph and Camera (YFOSC) on  
355 the Lijiang 2.4-m telescope of the Yunnan Observatories, and the DeVeny spectrograph mounted  
356 on the 4.3-m Discovery Channel Telescope (DCT). The Floyds spectra were reduced using the  
357 PyRAF-based `floydsspec` pipeline. The ALFOSC and DOLORES spectra were reduced using  
358 custom MATLAB pipelines. The LRIS spectra were reduced using the IDL `LPipe` pipeline. The  
359 DEIMOS spectrum was reduced using a modified version of the `DEEP2` pipeline<sup>44, 45</sup> combined  
360 with standard PyRAF and IDL routines for trace extraction, flux calibration and telluric correction.  
361 The DBSP spectrum was reduced using custom IRAF and IDL routines. The BFOSC, YFOSC and  
362 DeVeny spectra were reduced using standard IRAF procedures. All spectra are available for down-  
363 load via WISeREP<sup>46</sup>. No Na I D absorption is seen at the redshift of the host galaxy, indicating  
364 very low host-galaxy extinction at the supernova position.

365 We fit each iPTF14hls spectrum to a library of Type II supernovae (which includes a full set of  
366 SN 1999em spectra<sup>22</sup>) using Superfit<sup>47</sup>. We then calculate the average best-fit supernova phase,  
367 weighing all the possible fits by their corresponding fit scores. We repeat this process for cutouts  
368 of the iPTF14hls spectra centered around the  $H\alpha$ ,  $H\beta$ , and Fe II 5169Å features (separately).  
369 The weighted-average best-fit phases for each cutout are presented in Extended Data Figure 4.

370 iPTF14hls can be seen to evolve more slowly than other Type II supernovae by a factor of  $\approx 10$   
371 when considering the entire spectrum, as well as when considering the  $H\beta$  and the Fe II 5169Å  
372 features separately, and by a factor of 6–7 when considering the  $H\alpha$  emission feature separately.

373 Expansion velocities for different elements in iPTF14hls were measured by fitting a parabola  
374 around the minimum of the absorption feature of their respective P-Cygni profiles. The difference  
375 between the minimum of the best-fit parabola and the rest wavelength of the line was translated to  
376 an expansion velocity. The endpoints of each parabolic fit were chosen manually for each line, so  
377 that they would remain the same for all spectra. Uncertainties in the velocities were estimated by  
378 randomly varying these endpoints by  $\pm 5 \text{ \AA}$  around their original values.

379 **Is iPTF14hls Powered by Interaction?** As mentioned in the main text, interaction between su-  
380 pernova ejecta and a pre-existing dense CSM could cause an increase in luminosity. However,  
381 iPTF14hls does not display the spectral line profiles typically seen in such cases (Extended Data  
382 Figure 5).

383 In some interaction models the collision of the supernova ejecta and the CSM occurs outside the  
384 broad-line forming region, diluting the line emission. Focusing on the  $\approx 50\%$  luminosity increase  
385 of iPTF14hls between rest-frame day 207 and 232 after discovery (Fig. 1), we find that the spectra  
386 taken on day 207 and day 232 are identical up to a global normalization factor. This indicates that  
387 the increase in luminosity is equal at all wavelengths, in contrast to the expected line dilution from  
388 interaction (Extended Data Figure 6).

389 Additional possible indicators of interaction are strong X-ray and/or radio emission. We observed  
 390 the location of iPTF14hls with the X-Ray Telescope (XRT)<sup>48</sup> onboard the *Swift* satellite<sup>49</sup> on  
 391 2015 May 23.05. A total 4.9 ks of live exposure time was obtained on the source. We use on-  
 392 line analysis tools<sup>50, 51</sup> to search for X-ray emission at the location of iPTF14hls. No source is  
 393 detected with an upper limit on the 0.3–10.0 keV count rate of  $< 2.3 \times 10^{-3} \text{ ct s}^{-1}$ . Assum-  
 394 ing a power-law spectrum with a photon index of  $\Gamma = 2$  and a Galactic H column density<sup>52</sup>  
 395 of  $1.4 \times 10^{20} \text{ cm}^{-2}$ , this corresponds to an upper limit on the unabsorbed 0.3–10.0 keV flux of  
 396  $f_X < 8.4 \times 10^{-14} \text{ erg cm}^{-2} \text{ s}^{-1}$ . At the luminosity distance of iPTF14hls this corresponds to  
 397 a luminosity limit of  $L_X < 2.5 \times 10^{41} \text{ erg s}^{-1}$  (which is roughly  $10^{-2}$  of the peak bolometric  
 398 luminosity). The lack of X-ray emission disfavors strong interaction in iPTF14hls though some  
 399 interacting supernovae display X-ray emission fainter than the limit we deduce here<sup>53</sup>. We ob-  
 400 served iPTF14hls also with the Arcminute Microkelvin Imager Large Array (AMI-LA)<sup>54</sup> at 15  
 401 GHz on 2015 May 18.59, May 19.77, May 23.63, May 25.65, May 28.66, and May 31.62. 3C48  
 402 and J2035+1056 were used as the flux/bandpass and phase calibrators, respectively. RFI excision  
 403 and calibration of the raw data was done with a fully automated pipeline AMI-REDUCE<sup>55, 56</sup>. The  
 404 calibrated data for the supernova were imported into CASA and imaged independently for each  
 405 epoch into  $512 \times 512$  pixel maps ( $4''$  per pixel) using the `clean` task. A similar imaging scheme  
 406 was used for the concatenated data from all the epochs as well. The supernova was not detected on  
 407 any of the individual epochs, with  $3\sigma$  upper limits between 60–120  $\mu\text{Jy}$ . The combined  $3\sigma$  upper  
 408 limit is 36  $\mu\text{Jy}$ . There is a 5–10% absolute flux calibration uncertainty that we have not considered  
 409 in these upper limits. On 2016 Jun 10, iPTF14hls was observed with the VLA at 6.1 GHz. The

410 VLA data were reduced using standard CASA software routines where J0920+4441 and 3C286  
411 were used as phase and flux calibrators. No radio emission was observed at the supernova posi-  
412 tion to a  $3\sigma$  upper limit of  $21.3 \mu\text{Jy}$ . At the luminosity distance of iPTF14hls, this corresponds to  
413  $6.2 \times 10^{26} \text{ erg s}^{-1} \text{ Hz}^{-1}$ , which is fainter than the radio emission of most interacting supernovae<sup>53</sup>.

414 We conclude that iPTF14hls does not show any of the signatures seen in supernovae powered by  
415 interaction.

416 **Is iPTF14hls Powered by a Central Engine?** A central engine such as the spindown of a magnetar<sup>57, 12, 58</sup>  
417 or fallback accretion onto a black hole<sup>59, 13</sup> created after core collapse (assuming the material falling  
418 back has sufficient angular momentum to form a disk) could inject power to the supernova, al-  
419 though, as noted in the main text, this may fail to reproduce the observed iron and hydrogen line  
420 velocity difference. A magnetar (with an initial spin period of  $\approx 5\text{--}10$  ms and a magnetic field of  
421  $\approx (0.5\text{--}1) \times 10^{14}$  Gauss) can produce the observed average luminosity and timescale of iPTF14hls<sup>12</sup>.  
422 However, the analytical magnetar light curve required to fit the late-time decline overpredicts the  
423 early-time emission of iPTF14hls (Extended Data Fig. 2) and produces a smooth rather than vari-  
424 able light curve<sup>12, 13</sup>. For a black hole central engine, on the other hand, instabilities in the accretion  
425 flow might produce strong light-curve variability, as seen in active galactic nuclei<sup>20</sup>. In this case,  
426 the light curve is expected to eventually settle onto a  $t^{-5/3}$  decline rate<sup>21</sup> after the last instability.  
427 Such a decline rate is indeed observed for iPTF14hls starting on day  $\approx 450$  (Extended Data Fig.  
428 2), supporting a black hole power source.

429 We conclude that iPTF14hls does not show the expected signatures of magnetar power (using  
430 available analytical models), but might be consistent with black hole accretion power.

431 **Is iPTF14hls Assymmetric?** A possible explanation for the high luminosities and apparent emitted  
432 energy of iPTF14hls, as well as the discrepancy between its line-forming vs. blackbody radii, is  
433 strong assymetry in the explosion. Such assymetry would be indicated by a polarization signal.

434 We observed iPTF14hls with the Andalucia Faint Object Spectrograph and Camera (ALFOSC)  
435 mounted on the 2.5-m Nordic Optical Telescope (NOT) in polarimetric mode on 2015 Nov 03 in  
436 *R*-band, and Dec 15 in *V*-band (we also obtained observations on 2015 Oct 28 and Nov 14 but  
437 we discard them due to very poor observing conditions). We used a 1/2 wave plate in the FAPOL  
438 unit and a calcite plate mounted in the aperture wheel, and observed in 4 different retarder angles  
439 (0, 22.5, 45, 67.5 degrees). The data were reduced in a standard manner, using bias frames and  
440 flat-fields without the polarisation units in the light path. The field of view contains one bright star  
441 that can be used for calibration and for determining the interstellar polarisation (ISP) in the Galaxy.  
442 The low Galactic extinction towards iPTF14hls implies an expected ISP value of  $< 0.13\%$ <sup>60</sup>. To  
443 measure the fluxes we performed aperture photometry, and to compute the polarisation we followed  
444 standard procedures<sup>61</sup>. For our epoch with the best signal to noise (2015 Nov 03), we measure  
445  $P = 0.40 \pm 0.27\%$  for iPTF14hls and  $P = 0.17 \pm 0.09\%$  for the comparison star, in agreement  
446 with the ISP prediction. These results suggest that iPTF14hls is close to spherically symmetric,  
447 similar to what is observed for Type II-P supernovae during their plateau phase<sup>62</sup>. The 2015 Dec  
448 15 epoch yields a lower precision ( $P = 1.1 \pm 0.7\%$  for iPTF14hls and  $P = 0.80 \pm 0.23\%$  for the  
449 comparison star), but is still consistent with very low asphericity.

450 **Why are the Expansion Velocities of iPTF14hls so Perplexing?** In a supernova, the ejecta are  
451 in homologous expansion — that is, the radius of the ejecta at time  $t$  evolves as  $r = vt$ , with faster  
452 material at larger radii. Even for perfectly mixed ejecta, at any given time, spectral lines of different  
453 elements form in different regions. Specifically, the Fe lines are formed at smaller radii than the H  
454 lines and therefore display a lower velocity. This is also the case in iPTF14hls. As time passes and  
455 the ejecta expand and recombine, the line-forming region of each element moves inward in mass  
456 to a region where the outflow is slower. This is why, normally, the velocity of all lines is observed  
457 to decrease with time. Thus, following the line velocity over a wide range of time (and hence mass  
458 coordinates) provides a “scan” of the velocity profile over a large range of the ejecta. Although  
459 different lines are formed at different regions, all line-forming regions scan the velocity profile of  
460 the same ejecta. Therefore if there is a significant velocity gradient in the ejecta, we expect to see  
461 both a significant velocity difference between the Fe and H lines as well as significant evolution  
462 in the velocity of each line as the material expands. These two features are seen clearly in the  
463 typical case of SN 1999em (Extended Data Fig. 7). However, this is not the case in iPTF14hls.  
464 On the one hand there is a significant difference between the H and Fe line velocities, indicating  
465 a large velocity gradient in the ejecta. On the other hand, the velocity of each line shows almost  
466 no evolution in time between days 100 and 600 after discovery. If the line-forming material were  
467 ejected at discovery then this time span corresponds to a change by a factor of  $\approx 6$  in radius. In  
468 this case, the lack of observed velocity evolution indicates a very shallow velocity gradient in the  
469 ejecta, which is inconsistent with the large velocity difference between the lines. However, if the  
470 ejection of the line-forming material took place before discovery, then the relative change in radius

471 during the observations is small, indicating that the position of the line-forming region does not  
 472 change much, potentially solving the apparent contradiction.

473 **The Line-Forming Region of iPTF14hls** The nearly constant line velocities measured in iPTF14hls  
 474 suggest that the lines form in a massive shell, perhaps ejected prior to the explosion. Here we esti-  
 475 mate the mass and energetics required for such a shell to produce the observed line features.

476 Consider a uniform shell of mass  $M$  with a radius  $r$  and width  $\Delta r$ . The number density of hydrogen  
 477 atoms in the shell is

$$n_{\text{H}} = \frac{Y_{\text{H}} M}{\mu m_p 4\pi r^2 \Delta r} \quad (1)$$

478 where  $Y_{\text{H}} \approx 0.9$  is the number fraction of hydrogen and  $\mu \approx 1.34$  the mean atomic mass for solar  
 479 gas ( $m_p$  is the proton mass). In a rapidly expanding, homologous outflow ejected at a time  $t_{\text{ej}}$ , the  
 480 strength of a spectral line is characterized by the Sobolev optical depth approximation

$$\tau_{\text{sob}} = \frac{\pi e^2}{m_e c} n_l f t_{\text{ej}} \lambda_0 \quad (2)$$

481 where  $n_l$  is the number density of atoms in the lower level,  $f$  is the line oscillation strength,  $t_{\text{ej}}$   
 482 is the time since explosion, and  $\lambda_0$  is the line rest wavelength. For a line to produce a noticeable  
 483 absorption component in the spectra, it must have  $\tau_{\text{sob}} \gtrsim 1$ .

484 To estimate the populations in the lower level of the line transition (for the Balmer series this is  
 485 the  $n = 2$  level), we apply the nebular approximation<sup>63</sup>, which assumes the mean intensity of the  
 486 radiation field at a radius above a nearly blackbody photosphere is  $J_\nu(r) = W(r) B_\nu(T_{\text{bb}})$  where  
 487  $B_\nu$  is the Planck function,  $T_{\text{bb}}$  is the temperature of the photosphere, and  $W(r)$  is the geometrical



488 dilution factor of the radiation field:

$$W(r) = \frac{1}{2} \left[ 1 - \sqrt{1 - r_p^2/r^2} \right] \approx \frac{r_p^2}{4r^2} \quad (3)$$

489 Here,  $r_p$  is the photospheric radius and the last expression assumes  $r \gg r_p$ . For a two-level atom  
 490 subject to this radiation field, the number density in the  $n = 2$  excited state is

$$n_2 \approx n_1 W \frac{g_2}{g_1} e^{-\Delta E_{1,2}/kT} \quad (4)$$

491 where  $n_1, n_2$ , and  $g_1, g_2$  are (respectively) the number density and statistical weights of the  $n = 1$   
 492 and  $n = 2$  levels, and  $\Delta E_{1,2}$  is the energy difference between the levels.

493 Since essentially all of the hydrogen in the shell will be neutral and in the ground state,  $n_1 \approx n_H$ .

494 The Sobolev optical depth is then

$$\tau_{H\alpha} \approx \left[ \frac{\pi e^2}{m_e c} f \lambda_0 t_{ej} \right] \frac{Y_H M}{\mu m_p} \frac{r_p^2}{16\pi r^4 \Delta r} \frac{g_2}{g_1} e^{-\Delta E_{1,2}/kT} \quad (5)$$

495 Using  $g_1 = 2$ ,  $g_2 = 8$ ,  $\Delta E_{1,2} = 10.2 \text{ eV}$ ,  $\lambda_0 = 6563 \text{ \AA}$  (for the  $H\alpha$  transition), and  $f = 0.64$ , and  
 496 taking  $T = 6500 \text{ K}$ ,  $\Delta r = \Delta v t_{ej}$  and  $r = v t_{ej}$  gives

$$\tau_{H\alpha} \approx 0.96 \left[ \frac{M}{45 M_\odot} \right] \left[ \frac{600 \text{ days}}{t_{ej}} \right]^4 \left[ \frac{r_p}{1.5 \times 10^{15} \text{ cm}} \right]^2 \left[ \frac{6000 \text{ km s}^{-1}}{v} \right]^4 \left[ \frac{1000 \text{ km s}^{-1}}{\Delta v} \right] \quad (6)$$

497 Though approximate, this argument demonstrates that a shell with a mass of order a few tens  
 498 of solar masses is likely required for producing Balmer absorption lines throughout the  $\approx 600$ -  
 499 day duration of the iPTF14hls light curve. The corresponding kinetic energy of the outburst is  
 500  $\sim 10^{52}$  erg. In the case that the shell was ejected before the first iPTF14hls observations, the mass  
 501 and energy required would increase. However, the mass required to associate the line forming

502 region with the 1954 eruption would be  $\sim 10^7 M_\odot$ , and hence not reasonable, implying that the  
 503 line forming region was ejected in a separate, more recent, eruption.

504 For comparison, the electron-scattering optical depth of the shell is

$$\tau_{\text{es}} = n_{\text{H}} x_{\text{HII}} \sigma_T \Delta r \approx 0.77 x_{\text{HII}} \left[ \frac{M}{45 M_\odot} \right] \left[ \frac{600 \text{ days}}{t_{\text{ej}}} \right]^2 \left[ \frac{6000 \text{ km s}^{-1}}{v} \right]^4 \quad (7)$$

505 where  $\sigma_T$  is the Thomson cross-section and  $x_{\text{HII}}$  is the fraction of ionized hydrogen. The shell will  
 506 be largely neutral ( $x_{\text{HII}} \ll 1$ ), because the region where the radiation field is sufficient to ionize  
 507 hydrogen occurs at the photosphere,  $r_p$ , where the recombination front forms. The shell radius is  
 508 much larger than  $r_p$ , and so the radiation field is strongly diluted. Thus, while the shell can form  
 509 line features, it will be optically thin in the continuum and allow most of the pseudo-blackbody  
 510 continuum from the photosphere to pass through.

511 The velocity of  $6000 \text{ km s}^{-1}$  seen for  $\text{H}\alpha$  at day 600 after discovery, is seen for  $\text{H}\beta$  at day 200  
 512 after discovery. If we calculate the optical depth (Eq. 5) for  $\text{H}\beta$ , plugging in the parameters  
 513 for day  $200 + t_0$ , and equate it to that of  $\text{H}\alpha$  at day  $600 + t_0$  (where  $t_0$  is the offset between  
 514 the ejection of the shell and discovery), then we can solve for the ejection time  $t_0$ , assuming the  
 515 optical depth for  $\text{H}\alpha$  and  $\text{H}\beta$  were the same when each was observed at  $6000 \text{ km s}^{-1}$ , and that the  
 516 entire shell was ejected simultaneously. Using  $\lambda_0 = 4861 \text{ \AA}$  and  $f = 0.12$  for the  $\text{H}\beta$  transition,  
 517 we find  $t_0 \approx 100\text{--}200$  days (the main source of error is the uncertainty in the precise temperature  
 518 difference between the two epochs), meaning that the line-forming shell was ejected 100–200 days  
 519 before discovery. We have deep non-detection limits for part of this epoch (Extended Data Fig.  
 520 3) suggesting that that the ejection of the shell could have been a low-luminosity event. This

521 estimation of the ejection time, however, relies on many simplifying assumptions, so should be  
522 considered only as an approximation.

523 **An Historical Outburst at the Position of iPTF14hls** The Palomar Observatory Sky Survey  
524 (POSS)<sup>64</sup> observed the field of iPTF14hls on 1954 Feb. 23 in the blue and red filters. POSS-II<sup>65</sup>  
525 then re-observed the field on 1993 Jan. 2 in the blue filter and on 1995 Mar. 30 in the red filter. We  
526 obtained these images through the STScI Digitized Sky Survey and we find a source at the position  
527 of iPTF14hls in the blue image from POSS that is not present in the blue image from POSS-II  
528 (Extended Data Fig. 8). We do not see this source in either of the red images, but they are not as  
529 deep as the blue images (the limiting magnitude is roughly 20 for the red images compared to 21.1  
530 for the blue images)<sup>64</sup>.

531 We register the POSS blue image to the POSS-II blue image using the IRAF task `wregister`. We  
532 then use the `apphot` package in PyRAF, with a 3-pixel aperture, to measure the flux in six stars  
533 in the field near the position of iPTF14hls to determine a zero-point offset for the two images. We  
534 find an offset of  $0.132 \pm 0.050$  mag. We then perform the same measurement around the nucleus of  
535 the host galaxy of iPTF14hls and find an offset of 0.141 mag, consistent with the zero-point offset.  
536 Next we perform the same aperture photometry measurement at the position of iPTF14hls in both  
537 images. We find a magnitude difference of  $0.31 \pm 0.14$  over the host-galaxy level confirming the  
538 presence of an outburst in the 1954 image at the position of iPTF14hls at a  $2.2\sigma$  confidence level.  
539 Owing to the nonlinear nature of the photographic plates used in the two POSS surveys, as well  
540 as differences between the filters<sup>65</sup>, we cannot perform meaningful image subtraction between the  
541 POSS epochs to obtain more accurate photometric measurements. We consider this confidence

542 level to be a conservative estimate, the outburst can be seen clearly by eye in the images (Extended  
543 Data Fig. 8).

544 We calibrate the six stars used for the zero-point comparison to SDSS  $u$  plus  $g$ -band fluxes (the  
545 POSS blue filter roughly covers the SDSS  $u$  and  $g$  bands)<sup>64</sup> and find that the magnitude of the 1954  
546 outburst (after removing host-galaxy contribution) is  $20.4 \pm 0.1$  (stat)  $\pm 0.8$  (sys). The first error is  
547 statistical and due to photometric measurement uncertainties, while the second error is systematic  
548 and caused by the calibration to SDSS (the large error value is likely due to filter and detector  
549 differences between POSS and SDSS).

550 This corresponds to an absolute magnitude for the outburst of  $\approx -15.6$  at the luminosity distance  
551 of iPTF14hls (this is only a lower limit on the peak luminosity of the eruption, as we have only one  
552 epoch of observations). Such an eruption may be produced by the pulsational pair instability<sup>2, 3, 4, 5</sup>.  
553 Similar luminosity eruptions (though likely due to different instabilities) are inferred to be com-  
554 mon in Type II<sub>n</sub> supernova progenitors in the last year prior to explosion<sup>66</sup>. Spectra and broad-band  
555 colors are available for three such possible outbursts - a precursor to PTF10bjb<sup>66</sup>, PTF13efv (a pre-  
556 cursor to SNHunt275)<sup>67</sup> and the first 2012 outburst of SN 2009ip<sup>68</sup> - all of which display rather flat  
557 continuum emission, consistent with the limited color information we have for the 1954 outburst  
558 of iPTF14hls (i.e. the red non-detection limit being roughly 0.4 magnitudes brighter than the blue  
559 detection).

560 Given the host galaxy size of  $\sim 10$ – $100$  times the centroiding error of the outburst, and a typical  
561 supernova rate of  $\sim 100$  per galaxy per year, there is a few percent probability that the detected

562 outburst is an unrelated supernova that happened to occur at the position of iPTF14hls.

563 **The Rate of iPTF14hls-like Events** On 2014 Nov. 18, iPTF14hls was independently discovered  
564 by the Catalina Real-Time Transient Survey<sup>25</sup> as CSS141118:092034+504148, and more recently  
565 the event was reported to the Transient Name Server as AT 2016bse and Gaia16aog. The fact that  
566 it was discovered multiple times, but dismissed as a run of the mill SN II-P, is suggestive that  
567 similar events may have been missed in the past. We ourselves would not have noticed the unique  
568 properties of iPTF14hls had the iPTF survey scheduler not automatically continued to monitor the  
569 position of iPTF14hls. In addition, if iPTF14hls-like events are limited to low-mass galaxies, then  
570 targeted transient surveys would have missed them completely.

571 To our knowledge, iPTF14hls is the only supernova ever discovered to show such long-lived,  
572 slowly-evolving II-P-like emission. The PTF and iPTF surveys discovered 631 Type II supernovae,  
573 indicating that iPTF14hls-like events could be  $\sim 10^{-3} - 10^{-2}$  of the Type II supernova rate. Since  
574 luminous long-lived varying events could be easier to detect in transient surveys compared to  
575 normal supernovae, the true volumetric rate of iPTF14hls-like events could be much lower. On the  
576 other hand, we cannot rule out whether such events were discovered in the past but dismissed as  
577 normal Type II-P supernovae after one spectrum with no subsequent followup or as possible AGN  
578 due to the light curve behavior. It is therefore not possible to calculate a precise rate for iPTF14hls-  
579 like events based on this single discovery, but whatever the explosion channel, it is likely to be rare.  
580 Even so, the Large Synoptic Survey Telescope could find hundreds of iPTF14hls-like events in its  
581 decade-long survey of the transient sky (more so if iPTF14hls-like events are more common in the  
582 early Universe, as is indicated by the possible low-metallicity environment of iPTF14hls).

583 **The Host Galaxy of iPTF14hls** We obtained a spectrum of the host galaxy of iPTF14hls on 2015  
584 Dec 11 with the Low Resolution Imaging Spectrometer (LRIS)<sup>41</sup> mounted on the Keck I 10-m  
585 telescope. The spectrum was reduced using the standard techniques optimized for Keck+LRIS by  
586 the `CarPy` package in PyRAF, and flux calibrated to spectrophotometric standard stars obtained  
587 on the night of our observations in the same instrument configuration. The host galaxy spectrum,  
588 which is available for download via WISEREP<sup>46</sup>, shows clear detections of  $H\alpha$ ,  $H\beta$ , [O II] 3727Å  
589 and [O III] 4958,5007Å which we use to determine the redshift of 0.0344. A faint detection of  
590 [N II] 6583Å is also possible, but because the continuum is contaminated by broad  $H\alpha$  emission  
591 from the nearby supernova this feature is difficult to confirm. All of the lines are weak (equivalent  
592 width  $< 20\text{\AA}$ ) and no other lines are significantly detected. We extracted the fluxes of all lines  
593 by fitting Gaussians to their profiles (Extended Table 1), and calculated the metallicity by fitting<sup>69</sup>  
594 the line-strength ratios using several different diagnostics and calibrations (Extended Table 2). We  
595 find a range of metallicity estimates of  $12 + \log(\text{O}/\text{H}) = 8.3\text{--}8.6$ , corresponding to  $\approx 0.4\text{--}0.9 Z_{\odot}$   
596 (where  $Z_{\odot}$  is the solar metallicity)<sup>70</sup>. A low metallicity could help explain how the progenitor of  
597 iPTF14hls retained a very massive hydrogen envelope. Future more direct environment studies  
598 will be able to better probe the metallicity at the explosion site.

599 We fit the SDSS *ugriz* photometry of the host galaxy<sup>71</sup> with standard SED fitting techniques<sup>72</sup>  
600 using the BC03<sup>73</sup> stellar population synthesis models. Assuming a metallicity of  $0.5 Z_{\odot}$ , the best  
601 fit total stellar mass is  $3.2 \pm 0.5 \times 10^8 M_{\odot}$ , similar to that of the Small Magellanic Cloud.

- 602 23. Cao, Y., Nugent, P. E. & Kasliwal, M. M. Intermediate Palomar Transient Factory: Realtime  
604 Image Subtraction Pipeline. *eprint arXiv:1608.01006* (2016). URL [http://arxiv.org/](http://arxiv.org/abs/1608.01006)  
605 [abs/1608.01006](http://arxiv.org/abs/1608.01006). 1608.01006.
- 606 24. Shappee, B. J. *et al.* the Man Behind the Curtain: X-Rays Drive the Uv Through Nir  
607 Variability in the 2013 Active Galactic Nucleus Outburst in Ngc 2617. *The Astrophys-*  
608 *ical Journal* **788**, 48 (2014). URL <http://arxiv.org/abs/1310.2241><http://dx.doi.org/10.1088/0004-637X/788/1/48>[http://adsabs.harvard.](http://adsabs.harvard.edu/abs/2014ApJ...788...48S)  
609 [edu/abs/2014ApJ...788...48S](http://adsabs.harvard.edu/abs/2014ApJ...788...48S). 1310.2241.
- 611 25. Drake, A. J. *et al.* First Results from the Catalina Real-time Transient Survey. *The Astrophys-*  
612 *ical Journal* **696**, 870–884 (2009). URL <http://arxiv.org/abs/0809.1394><http://dx.doi.org/10.1088/0004-637X/696/1/870>. 0809.1394.
- 614 26. Cenko, S. B. *et al.* The Automated Palomar 60 Inch Telescope. *Publications of the Astronom-*  
615 *ical Society of the Pacific* **118**, 1396–1406 (2006). 0608323.
- 616 27. Brown, T. M. *et al.* Las Cumbres Observatory Global Telescope Network. *Publications*  
617 *of the Astronomical Society of Pacific, Volume 125, Issue 931, pp. 1031-1055* (2013). **125**,  
618 1031–1055 (2013). URL <http://arxiv.org/abs/1305.2437>[http://dx.doi.](http://dx.doi.org/10.1086/673168)  
619 [org/10.1086/673168](http://dx.doi.org/10.1086/673168). 1305.2437.
- 620 28. Huang, F. *et al.* The photometric system of the Tsinghua-NAOC 80-cm telescope at NAOC  
621 Xinglong Observatory. *Research in Astronomy and Astrophysics, Volume 12, Issue 11, pp.*  
622 *1585-1596* (2012). **12**, 1585–1596 (2012). 1205.6529.

- 623 29. Laher, R. R. *et al.* IPAC Image Processing and Data Archiving for the Palomar Transient  
624 Factory. *Publications of the Astronomical Society of the Pacific* **126**, 674–710 (2014). 1404.  
625 1953.
- 626 30. Sullivan, M. *et al.* Photometric Selection of High-Redshift Type Ia Supernova Candidates.  
627 *The Astronomical Journal* **131**, 960–972 (2006). 0510857.
- 628 31. Ahn, C. P. *et al.* The Tenth Data Release of the Sloan Digital Sky Survey: First Spectroscopic  
629 Data from the SDSS-III Apache Point Observatory Galactic Evolution Experiment. *The As-*  
630 *trophysical Journal Supplement Series* **211** (2014). 1307.7735.
- 631 32. Fremling, C. *et al.* PTF12os and iPTF13bvn. Two stripped-envelope supernovae from low-  
632 mass progenitors in NGC 5806. *eprint arXiv:1606.03074* (2016). URL [http://arxiv.](http://arxiv.org/abs/1606.03074)  
633 [org/abs/1606.03074](http://arxiv.org/abs/1606.03074). 1606.03074.
- 634 33. Jenness, T. & Economou, F. ORAC-DR: A generic data reduction pipeline infrastructure.  
635 *Astronomy and Computing* **9**, 40–48 (2015). 1410.7509.
- 636 34. Valenti, S. *et al.* The diversity of Type II supernova versus the similarity in their progenitors.  
637 *Monthly Notices of the Royal Astronomical Society, Volume 459, Issue 4, p.3939-3962* **459**,  
638 3939–3962 (2016). URL <http://arxiv.org/abs/1603.08953>[http://dx.doi.](http://dx.doi.org/10.1093/mnras/stw870)  
639 [org/10.1093/mnras/stw870](http://dx.doi.org/10.1093/mnras/stw870). 1603.08953.
- 640 35. Henden, A. A., Welch, D. L., Terrell, D. & Levine, S. E. The AAVSO Photometric All-Sky  
641 Survey (APASS) (2009).



- 642 36. Aihara, H. *et al.* The Eighth Data Release of the Sloan Digital Sky Survey: First Data from  
643 SDSS-III. *The Astrophysical Journal Supplement Series* **193** (2011). 1101.1559.
- 644 37. Ahn, C. P. *et al.* The Ninth Data Release of the Sloan Digital Sky Survey: First Spec-  
645 troscopic Data from the SDSS-III Baryon Oscillation Spectroscopic Survey. *The Astro-*  
646 *physical Journal Supplement, Volume 203, Issue 2, article id. 21, 13 pp.* (2012). **203**  
647 (2012). URL <http://arxiv.org/abs/1207.7137>[http://dx.doi.org/10.](http://dx.doi.org/10.1088/0067-0049/203/2/21)  
648 [1088/0067-0049/203/2/21](http://dx.doi.org/10.1088/0067-0049/203/2/21). 1207.7137.
- 649 38. Chonis, T. S. & Gaskell, C. M. Setting UBVRI Photometric Zero-Points Using Sloan Digital  
650 Sky Survey ugriz Magnitudes. *The Astronomical Journal, Volume 135, Issue 1, pp. 264-267*  
651 (2008). **135**, 264–267 (2008). 0710.5801.
- 652 39. Schlafly, E. F. & Finkbeiner, D. P. Measuring Reddening with SDSS Stellar Spectra and  
653 Recalibrating SFD. *The Astrophysical Journal, Volume 737, Issue 2, article id. 103, 13 pp.*  
654 (2011). **737** (2011). URL <http://arxiv.org/abs/1012.4804>[http://dx.doi.](http://dx.doi.org/10.1088/0004-637X/737/2/103)  
655 [org/10.1088/0004-637X/737/2/103](http://dx.doi.org/10.1088/0004-637X/737/2/103). 1012.4804.
- 656 40. Foreman-Mackey, D., Hogg, D. W., Lang, D. & Goodman, J. emcee: The MCMC Ham-  
657 mer. *Publications of the Astronomical Society of Pacific, Volume 125, Issue 925, pp. 306-*  
658 *312* (2013). **125**, 306–312 (2012). URL <http://arxiv.org/abs/1202.3665>[http:](http://dx.doi.org/10.1086/670067)  
659 [//dx.doi.org/10.1086/670067](http://dx.doi.org/10.1086/670067). 1202.3665.
- 660 41. Oke, J. B. *et al.* The Keck Low-Resolution Imaging Spectrometer. *Publications of the*  
661 *Astronomical Society of the Pacific* **107**, 375 (1995). URL <http://www.jstor.org/>

662       stable/10.2307/40680546.

- 663 42. Faber, S. M. *et al.* The DEIMOS spectrograph for the Keck II Telescope: integration and  
664 testing. In Iye, M. & Moorwood, A. F. M. (eds.) *Instrument Design and Performance for*  
665 *Optical/Infrared Ground-based Telescopes. Edited by Iye, Masanori; Moorwood, Alan F.*  
666 *M. Proceedings of the SPIE, Volume 4841, pp. 1657-1669 (2003).*, vol. 4841, 1657–1669  
667 (2003). URL <http://proceedings.spiedigitallibrary.org/proceeding.aspx?articleid=874397>.
- 669 43. Oke, J. B. & Gunn, J. E. An Efficient Low Resolution and Moderate Resolution Spectrograph  
670 for the Hale Telescope. *Publications of the Astronomical Society of the Pacific* **94**, 586 (1982).  
671 URL <http://www.jstor.org/stable/10.2307/40677999>.
- 672 44. Cooper, M. C., Newman, J. A., Davis, M., Finkbeiner, D. P. & Gerke, B. F. spec2d: DEEP2  
673 DEIMOS Spectral Pipeline. *Astrophysics Source Code Library, record ascl:1203.003* (2012).
- 674 45. Newman, J. A. *et al.* The DEEP2 Galaxy Redshift Survey: Design, Observations, Data Re-  
675 duction, and Redshifts. *The Astrophysical Journal Supplement, Volume 208, Issue 1, article*  
676 *id. 5, 57 pp. (2013).* **208** (2012). URL <http://arxiv.org/abs/1203.3192>  
677 <http://dx.doi.org/10.1088/0067-0049/208/1/5.1203.3192>.
- 678 46. Yaron, O. & Gal-Yam, A. WISEREP - An Interactive Supernova Data Repository. *Pub-*  
679 *lications of the Astronomical Society of Pacific, Volume 124, Issue 917, pp. 668-681 (2012).*  
680 **124**, 668–681 (2012). URL <http://arxiv.org/abs/1204.1891>  
681 <http://dx.doi.org/10.1086/666656>. 1204.1891.

- 682 47. Howell, D. A. *et al.* Gemini Spectroscopy of Supernovae from SNLS: Improving High  
683 Redshift SN Selection and Classification. *The Astrophysical Journal*, Volume 634, Issue 2,  
684 *pp.* 1190-1201. **634**, 1190–1201 (2005). URL [http://arxiv.org/abs/astro-ph/](http://arxiv.org/abs/astro-ph/0509195)  
685 [0509195](http://arxiv.org/abs/astro-ph/0509195)<http://dx.doi.org/10.1086/497119>. 0509195.
- 686 48. Burrows, D. N. *et al.* The Swift X-ray Telescope. *Space Science Reviews* **120**, 165–195  
687 (2005). URL <http://arxiv.org/abs/astro-ph/0508071>[http://dx.doi.](http://dx.doi.org/10.1007/s11214-005-5097-2)  
688 [org/10.1007/s11214-005-5097-2](http://dx.doi.org/10.1007/s11214-005-5097-2). 0508071.
- 689 49. Gehrels, N. *et al.* The Swift GammaRay Burst Mission. *The Astrophysical Journal* **611**, 1005–  
690 1020 (2004). URL <http://stacks.iop.org/0004-637X/611/i=2/a=1005>.
- 691 50. Evans, P. A. *et al.* An online repository of Swift/XRT light curves of GRBs. *Astronomy and*  
692 *Astrophysics* **469**, 379–385 (2007). URL <http://arxiv.org/abs/0704.0128>[http:](http://dx.doi.org/10.1051/0004-6361:20077530)  
693 [//dx.doi.org/10.1051/0004-6361:20077530](http://dx.doi.org/10.1051/0004-6361:20077530). 0704.0128.
- 694 51. Evans, P. A. *et al.* Methods and results of an automatic analysis of a complete sample of  
695 Swift-XRT observations of GRBs. *Monthly Notices of the Royal Astronomical Society* **397**,  
696 1177–1201 (2009). URL <http://arxiv.org/abs/0812.3662>[http://dx.doi.](http://dx.doi.org/10.1111/j.1365-2966.2009.14913.x)  
697 [org/10.1111/j.1365-2966.2009.14913.x](http://dx.doi.org/10.1111/j.1365-2966.2009.14913.x). 0812.3662.
- 698 52. Willingale, R., Starling, R. L. C., Beardmore, A. P., Tanvir, N. R. & O’Brien, P. T. Cal-  
699 ibration of X-ray absorption in our Galaxy. *Monthly Notices of the Royal Astronomi-*  
700 *cal Society* **431**, 394–404 (2013). URL <http://arxiv.org/abs/1303.0843>[http:](http://dx.doi.org/10.1093/mnras/stt175)  
701 [//dx.doi.org/10.1093/mnras/stt175](http://dx.doi.org/10.1093/mnras/stt175). 1303.0843.

- 702 53. Margutti, R. *et al.* Ejection of the massive Hydrogen-rich envelope timed with the collapse  
703 of the stripped SN2014C. *eprint arXiv:1601.06806* (2016). URL [http://arxiv.org/  
704 abs/1601.06806](http://arxiv.org/abs/1601.06806). 1601.06806.
- 705 54. Zwart, J. T. L. *et al.* The Arcminute Microkelvin Imager. *Monthly Notices of the  
706 Royal Astronomical Society, Volume 391, Issue 4, pp. 1545-1558*. **391**, 1545–1558 (2008).  
707 URL <http://arxiv.org/abs/0807.2469>[http://dx.doi.org/10.1111/j.  
708 1365-2966.2008.13953.x](http://dx.doi.org/10.1111/j.1365-2966.2008.13953.x). 0807.2469.
- 709 55. Davies, M. L. *et al.* Follow-up observations at 16 and 33 GHz of extragalactic  
710 sources from WMAP 3-year data: I - Spectral properties. *Monthly Notices of the  
711 Royal Astronomical Society, Volume 400, Issue 2, pp. 984-994*. **400**, 984–994 (2009).  
712 URL <http://arxiv.org/abs/0907.3707>[http://dx.doi.org/10.1111/j.  
713 1365-2966.2009.15518.x](http://dx.doi.org/10.1111/j.1365-2966.2009.15518.x). 0907.3707.
- 714 56. Perrott, Y. C. *et al.* AMI Galactic Plane Survey at 16 GHz: I – Observing, mapping and source  
715 extraction. *Monthly Notices of the Royal Astronomical Society, Volume 429, Issue 4, p.3330-  
716 3340* **429**, 3330–3340 (2013). URL <http://arxiv.org/abs/1208.5343>[http://  
717 dx.doi.org/10.1093/mnras/sts589.1208.5343](http://dx.doi.org/10.1093/mnras/sts589.1208.5343).
- 718 57. Ostriker, J. P. & Gunn, J. E. On the Nature of Pulsars. I. Theory. *The Astrophysical Journal*  
719 **157**, 1395 (1969). URL <http://adsabs.harvard.edu/doi/10.1086/150160>.
- 720 58. Woosley, S. E. Bright Supernovae From Magnetar Birth. *The Astrophysical Journal* **719**,  
721 L204–L207 (2010). URL <http://adsabs.harvard.edu/abs/2010ApJ...719L>.

722

204W.

723

59. Colgate, S. A. Neutron-Star Formation, Thermonuclear Supernovae, and Heavy-Element

724

Reimplosion. *The Astrophysical Journal* **163**, 221 (1971). URL [http://adsabs.](http://adsabs.harvard.edu/doi/10.1086/150760)

725

[harvard.edu/doi/10.1086/150760](http://adsabs.harvard.edu/doi/10.1086/150760).

726

60. Serkowski, K., Mathewson, D. L. & Ford, V. L. Wavelength dependence of interstellar polar-

727

ization and ratio of total to selective extinction. *The Astrophysical Journal* **196**, 261 (1975).

728

URL <http://adsabs.harvard.edu/doi/10.1086/153410>.

729

61. Patat, F. & Romaniello, M. Error Analysis for Dual-Beam Optical Linear Polarimetry. *The*

730

*Publications of the Astronomical Society of the Pacific*, Volume 118, Issue 839, pp. 146-161.

731

**118**, 146–161 (2006). URL <http://arxiv.org/abs/astro-ph/0509153><http://dx.doi.org/10.1086/497581>.

732

0509153.

733

62. Leonard, D. C. & Filippenko, A. V. Spectropolarimetry of the Type II Supernovae 1997ds,

734

1998A, and 1999gi. *The Publications of the Astronomical Society of the Pacific*, Volume 113,

735

Issue 786, pp. 920-936. **113**, 920–936 (2001). 0105295.

736

63. Abbott, D. C. & Lucy, L. B. Multiline transfer and the dynamics of stellar winds. *The As-*

737

*trophysical Journal* **288**, 679 (1985). URL [http://adsabs.harvard.edu/doi/10.](http://adsabs.harvard.edu/doi/10.1086/162834)

738

[1086/162834](http://adsabs.harvard.edu/doi/10.1086/162834).

739

64. Minkowski, R. L. & Abell, G. O. The National Geographic Society-Palomar Observatory Sky

740

Survey. *Basic Astronomical Data: Stars and stellar systems*, edited by K. A. Strand. Published

741

by the University of Chicago Press, Chicago, IL USA, 1968, p.481 481 (1963).

- 742 65. Reid, I. N. *et al.* The second Palomar Sky Survey. *Publications of the Astronomical Society*  
743 *of the Pacific* **103**, 661 (1991). URL [http://www.jstor.org/stable/10.2307/](http://www.jstor.org/stable/10.2307/40651696)  
744 40651696.
- 745 66. Ofek, E. O. *et al.* Precursors prior to Type II<sub>n</sub> supernova explosions are common: precursor  
746 rates, properties, and correlations. *The Astrophysical Journal*, Volume 789, Issue 2, article  
747 *id. 104*, 15 pp. (2014). **789** (2014). URL <http://arxiv.org/abs/1401.5468><http://dx.doi.org/10.1088/0004-637X/789/2/104>. 1401.5468.  
748
- 749 67. Ofek, E. O. *et al.* PTF13efv An Outburst 500 Days Prior to the SN Hunt  
750 275 Explosion and its Radiative Efficiency. *The Astrophysical Journal* **824**,  
751 6 (2016). URL [http://stacks.iop.org/0004-637X/824/i=1/a=6?key=](http://stacks.iop.org/0004-637X/824/i=1/a=6?key=crossref.00771ff6ff8d40ebf094f40e98f1d67c)  
752 [crossref.00771ff6ff8d40ebf094f40e98f1d67c](http://stacks.iop.org/0004-637X/824/i=1/a=6?key=crossref.00771ff6ff8d40ebf094f40e98f1d67c).
- 753 68. Fraser, M. *et al.* SN 2009ip a la PESSTO: No Evidence for Core-Collapse Yet. *Monthly*  
754 *Notices of the Royal Astronomical Society*, Volume 433, Issue 2, p.1312-1337 **433**, 1312–  
755 1337 (2013). URL <http://arxiv.org/abs/1303.3453>[http://dx.doi.org/](http://dx.doi.org/10.1093/mnras/stt813)  
756 [10.1093/mnras/stt813](http://dx.doi.org/10.1093/mnras/stt813). 1303.3453.
- 757 69. Bianco, F. B. *et al.* Monte Carlo Method for Calculating Oxygen Abundances and Their  
758 Uncertainties from Strong-Line Flux Measurements. *Astronomy and Computing*, Volume 16,  
759 p. 54-66. **16**, 54–66 (2016). URL <http://arxiv.org/abs/1505.06213>. 1505.  
760 06213.

- 761 70. Asplund, M., Grevesse, N., Sauval, A. J. & Scott, P. The chemical composition of the  
762 Sun. *Annual Review of Astronomy & Astrophysics*, vol. 47, Issue 1, pp.481-522 **47**, 481–  
763 522 (2009). URL <http://arxiv.org/abs/0909.0948>[http://dx.doi.org/](http://dx.doi.org/10.1146/annurev.astro.46.060407.145222.0909.0948)  
764 [10.1146/annurev.astro.46.060407.145222.0909.0948](http://dx.doi.org/10.1146/annurev.astro.46.060407.145222.0909.0948).
- 765 71. Alam, S. *et al.* The Eleventh and Twelfth Data Releases of the Sloan Digital Sky Survey:  
766 Final Data from SDSS-III. *The Astrophysical Journal Supplement Series*, Volume 219, Is-  
767 sue 1, article id. 12, 27 pp. (2015). **219** (2015). URL [http://arxiv.org/abs/1501.](http://arxiv.org/abs/1501.00963)  
768 [00963](http://dx.doi.org/10.1088/0067-0049/219/1/12.1501.00963)<http://dx.doi.org/10.1088/0067-0049/219/1/12.1501.00963>.
- 769 72. Perley, D. A. *et al.* A Population of Massive, Luminous Galaxies Hosting Heavily Dust-  
770 Obscured Gamma-Ray Bursts: Implications for the Use of GRBs as Tracers of Cosmic  
771 Star Formation. *The Astrophysical Journal*, Volume 778, Issue 2, article id. 128, 35 pp.  
772 (2013). **778** (2013). URL <http://arxiv.org/abs/1301.5903>[http://dx.doi.](http://dx.doi.org/10.1088/0004-637X/778/2/128.1301.5903)  
773 [org/10.1088/0004-637X/778/2/128.1301.5903](http://dx.doi.org/10.1088/0004-637X/778/2/128.1301.5903).
- 774 73. Bruzual, G. & Charlot, S. Stellar population synthesis at the resolution of 2003. *Monthly*  
775 *Notices of the Royal Astronomical Society*, Volume 344, Issue 4, pp. 1000-1028. **344**, 1000–  
776 1028 (2003). URL <http://arxiv.org/abs/astro-ph/0309134>[http://dx.](http://dx.doi.org/10.1046/j.1365-8711.2003.06897.x.0309134)  
777 [doi.org/10.1046/j.1365-8711.2003.06897.x.0309134](http://dx.doi.org/10.1046/j.1365-8711.2003.06897.x.0309134).
- 778 74. Nagao, T., Maiolino, R. & Marconi, A. Gas metallicity diagnostics in star-forming galax-  
779 ies. *Astronomy and Astrophysics*, Volume 459, Issue 1, November III 2006, pp.85-101

- 780 **459**, 85–101 (2006). URL <http://arxiv.org/abs/astro-ph/0603580><http://dx.doi.org/10.1051/0004-6361:20065216>. 0603580.
- 781
- 782 75. Denicolo, G., Terlevich, R. & Terlevich, E. New light on the search for low metallicity  
783 galaxies I. The N2 method. *Monthly Notices of the Royal Astronomical Society, Volume 330,*  
784 *Issue 1, pp. 69-74.* **330**, 69–74 (2002). URL [http://arxiv.org/abs/astro-ph/](http://arxiv.org/abs/astro-ph/0110356)  
785 [0110356http://dx.doi.org/10.1046/j.1365-8711.2002.05041.x](http://dx.doi.org/10.1046/j.1365-8711.2002.05041.x).  
786 0110356.
- 787 76. Pettini, M. & Pagel, B. E. J. [O III]/[N II] as an Abundance Indicator at High Redshift.  
788 *Monthly Notices of the Royal Astronomical Society, Volume 348, Issue 3, pp. L59-L63.*  
789 **348**, L59–L63 (2004). URL <http://arxiv.org/abs/astro-ph/0401128><http://dx.doi.org/10.1111/j.1365-2966.2004.07591.x>. 0401128.
- 790
- 791 77. Maiolino, R. *et al.* AMAZE. I. The evolution of the mass-metallicity relation at  $z > 3$ .  
792 *Astronomy and Astrophysics, Volume 488, Issue 2, 2008, pp.463-479* **488**, 463–479  
793 (2008). URL <http://arxiv.org/abs/0806.2410>[http://dx.doi.org/10.](http://dx.doi.org/10.1051/0004-6361:200809678)  
794 [1051/0004-6361:200809678](http://dx.doi.org/10.1051/0004-6361:200809678). 0806.2410.
- 795 78. Marino, R. A. *et al.* The O3N2 and N2 abundance indicators revisited: improved calibra-  
796 tions based on CALIFA and Te-based literature data. *Astronomy & Astrophysics, Volume*  
797 *559, id.A114, 12 pp.* **559** (2013). URL <http://arxiv.org/abs/1307.5316><http://dx.doi.org/10.1051/0004-6361/201321956>. 1307.5316.
- 798

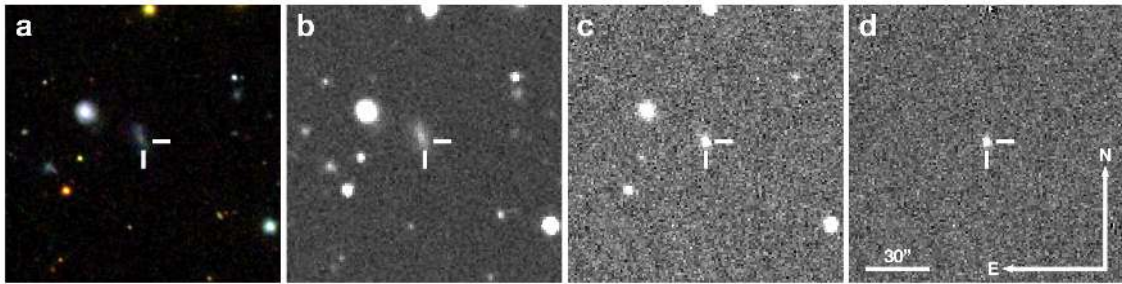


- 799 79. Kobulnicky, H. A. & Kewley, L. J. Metallicities of 0.3. *The Astrophysical Journal*, Vol-  
800 *ume 617, Issue 1, pp. 240-261. 617*, 240–261 (2004). URL [http://arxiv.org/abs/](http://arxiv.org/abs/astro-ph/0408128)  
801 [astro-ph/0408128](http://arxiv.org/abs/astro-ph/0408128)<http://dx.doi.org/10.1086/425299>. 0408128.
- 802 80. Kewley, L. J. & Dopita, M. A. Using Strong Lines to Estimate Abundances in Extragalactic  
803 HII Regions and Starburst Galaxies. *The Astrophysical Journal Supplement Series, Volume*  
804 *142, Issue 1, pp. 35-52. 142*, 35–52 (2002). URL [http://arxiv.org/abs/astro-ph/](http://arxiv.org/abs/astro-ph/0206495)  
805 [0206495](http://arxiv.org/abs/astro-ph/0206495)<http://dx.doi.org/10.1086/341326>. 0206495.

806

### Extended Data

807



808

**Extended Data Figure 1** The discovery and environment of iPTF14hls: (a) SDSS image cen-

809

tered at the position of iPTF14hls. (b) Palomar 48-inch deep coadded pre-discovery reference

810

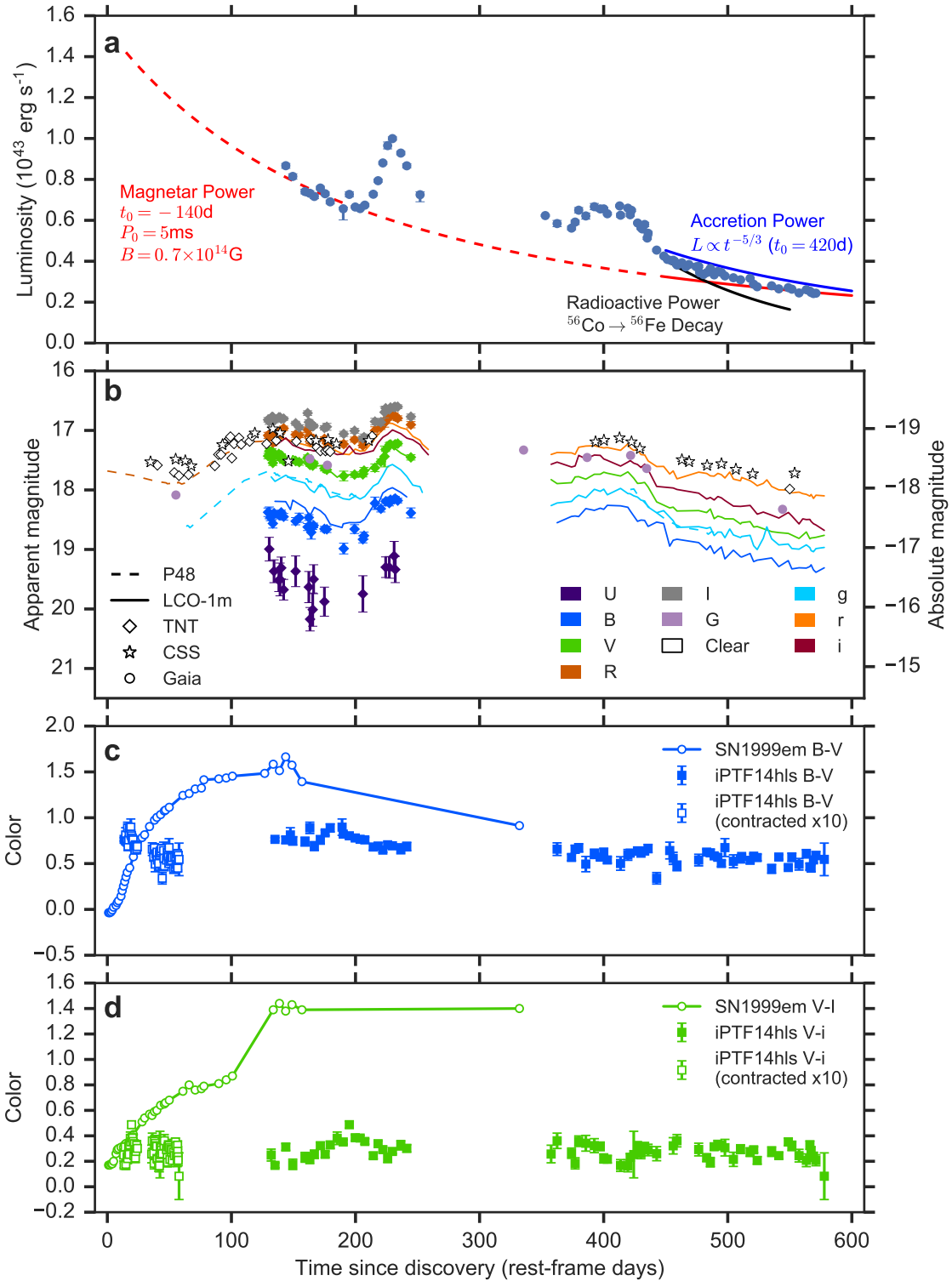
image. (c) Palomar 48-inch discovery image of iPTF14hls. (d) The result of subtracting the ref-

811

erence image from the discovery image. The position of iPTF14hls is indicated by tick marks in

812

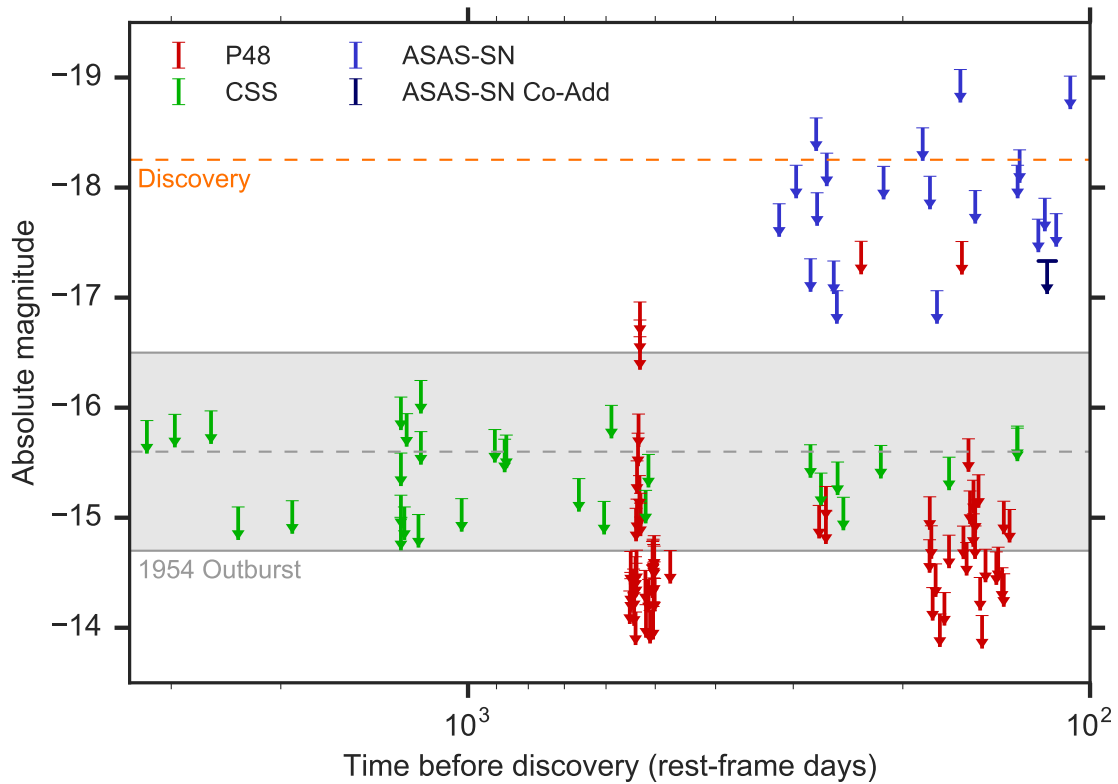
each image.



813

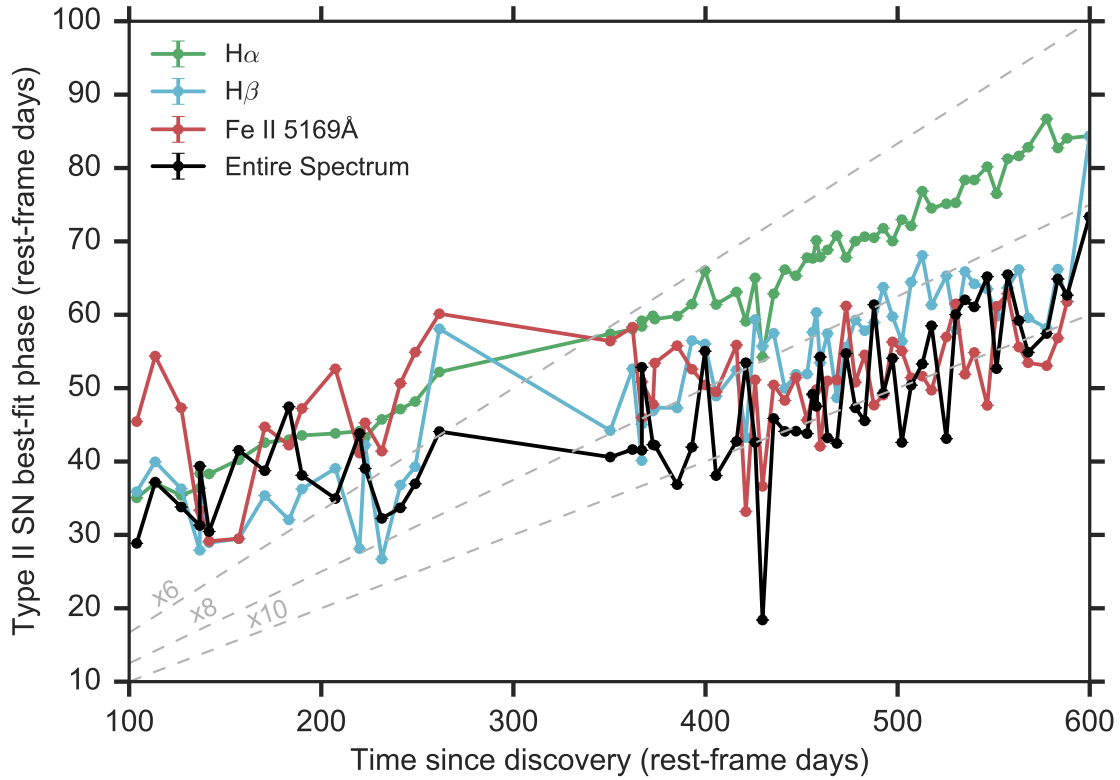
814 **Extended Data Figure 2** The bolometric light curve of iPTF14hls (a) deduced from the black-

815 body fits shows a late-time decline rate which is slower than the radioactive decay of  $^{56}\text{Co}$  (black),  
816 but consistent with both accretion power (blue;  $t_0$  is the onset of accretion at the last peak) and  
817 magnetar spindown power (red;  $t_0$  is the formation time of the magnetar,  $P_0$  is the initial spin pe-  
818 riod and  $B$  is the magnetic field in this simple analytic model). The magnetar model, however, is  
819 not consistent with the luminosity during the first 100 days, as implied by the P48, CSS and Gaia  
820 observations **(b)**, unless the early-time magnetar emission is significantly adiabatically degraded.  
821 TNT photometry of iPTF14hls and publicly available CSS and Gaia photometry **(b)**, not presented  
822 in Figure 1. Data from the P48 (dashed lines) and the LCO 1-m telescope (solid lines) presented  
823 in Figure 1 are shown for comparison. Photometric points from the same day, instrument, and  
824 filter are averaged for clarity. Error bars, available only for the TNT data, denote  $1\sigma$  uncertainties.  
825 The  $B-V$  **(c)** and  $V-I_i$  **(d)** color evolution of iPTF14hls from the LCO 1-m data (filled squares) dif-  
826 fers from that of the normal Type II-P SN 1999em (empty circles)<sup>22</sup>, even when contracting the  
827 iPTF14hls data by a factor of 10 in time (empty squares) to compensate for the slowed down  
828 evolution observed in its spectra compared to normal II-P supernovae.



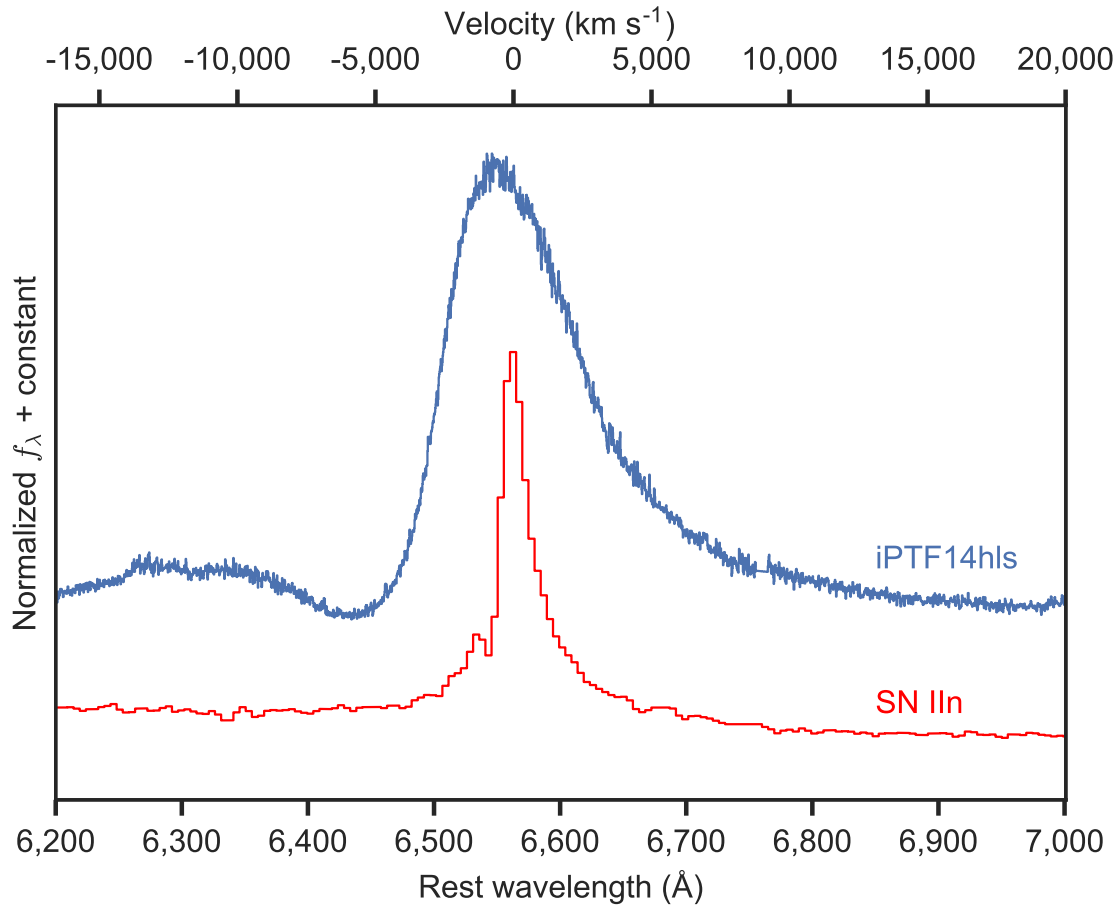
829

830 **Extended Data Figure 3** Pre-explosion nondetection limits for iPTF14hls from P48 (*R* band,  $3\sigma$   
 831 nondetections), CSS (unfiltered, obtained via the CSS website) and ASAS-SN (*V*-band,  $3\sigma$  non-  
 832 detections — the dark-blue arrow is a deep coadd of the three images taken during the time range  
 833 denoted by the horizontal line in the marker). The dashed line denotes the discovery magnitude  
 834 and the shaded region denotes the 1954 outburst magnitude and its uncertainty.



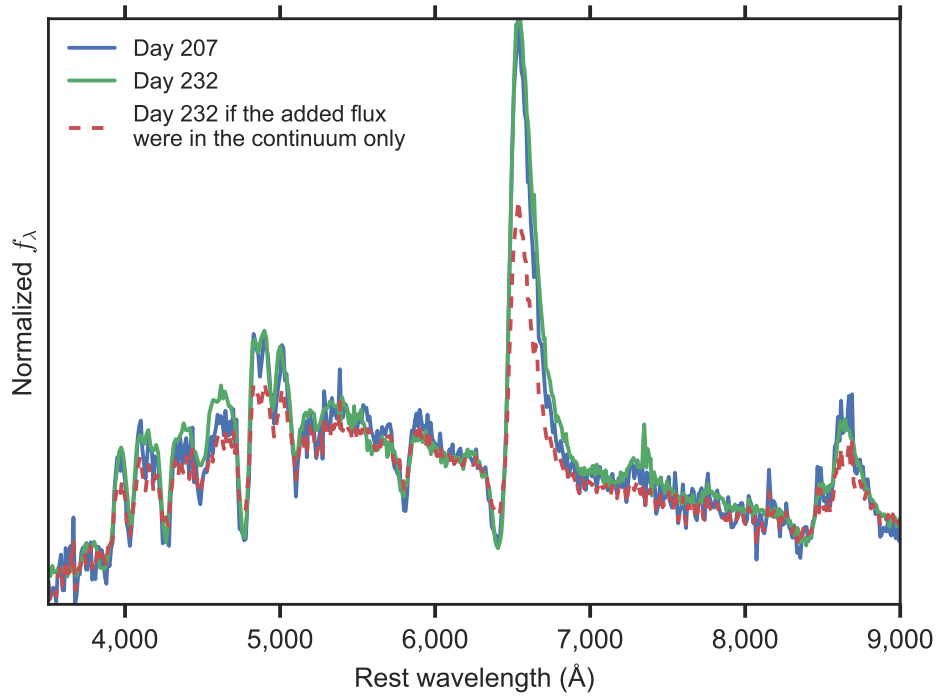
835

836 **Extended Data Figure 4** Weighted average best-fit phase of iPTF14hls spectra from Superfit<sup>47</sup>,  
 837 compared to the true spectral phase, when fitting the entire spectrum (black) or only certain line  
 838 regions as noted. The dashed lines denote constant ratios between the observed and best-fit  
 839 phases (assuming the explosion happened at discovery). The spectra of iPTF14hls are a factor of  
 840  $\approx 6$ –10 slower evolving compared to other Type II supernovae.



841

842 **Extended Data Figure 5** The  $H\alpha$  region in our highest-resolution spectrum of iPTF14hls taken  
 843 on 2016 June 4 using DEIMOS on Keck II (blue), expressed in terms of normalized flux density as  
 844 a function of rest-frame wavelength (bottom axis), compared to the interaction-powered Type IIn  
 845 supernova 2005cl<sup>18</sup> (red). The top axis is the corresponding velocity of  $H\alpha$ . iPTF14hls shows no  
 846 signs of the narrow emission or narrow P-Cygni features seen in interacting supernovae.

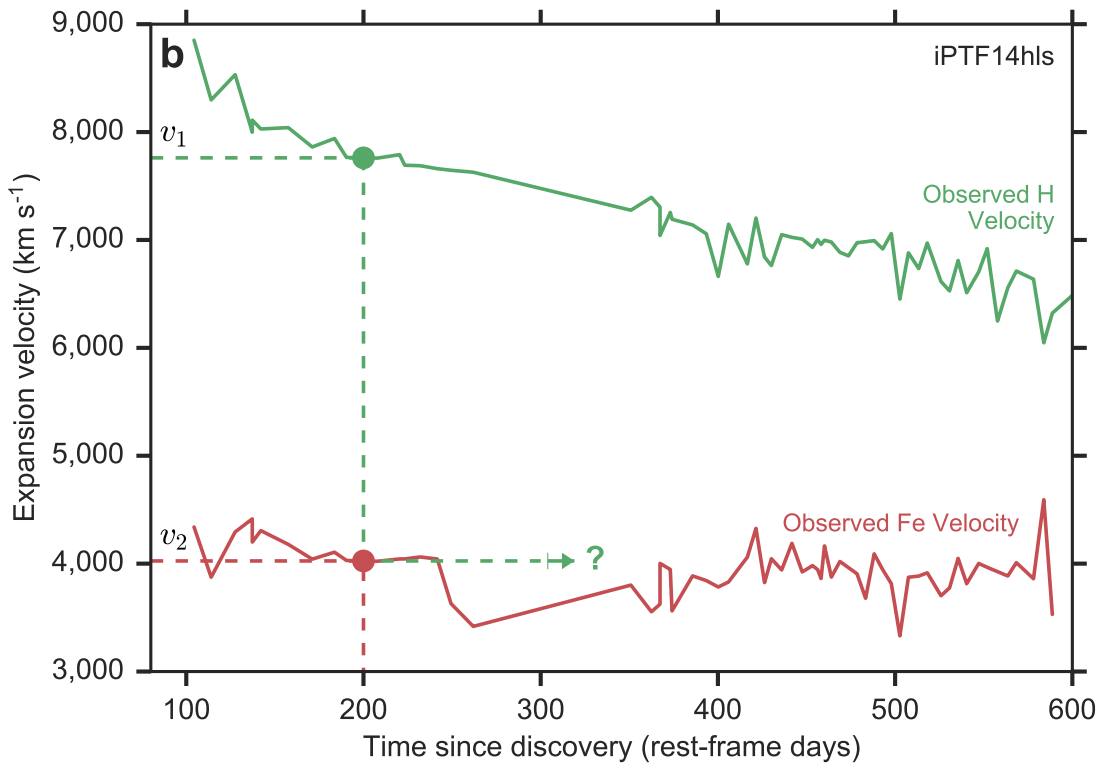
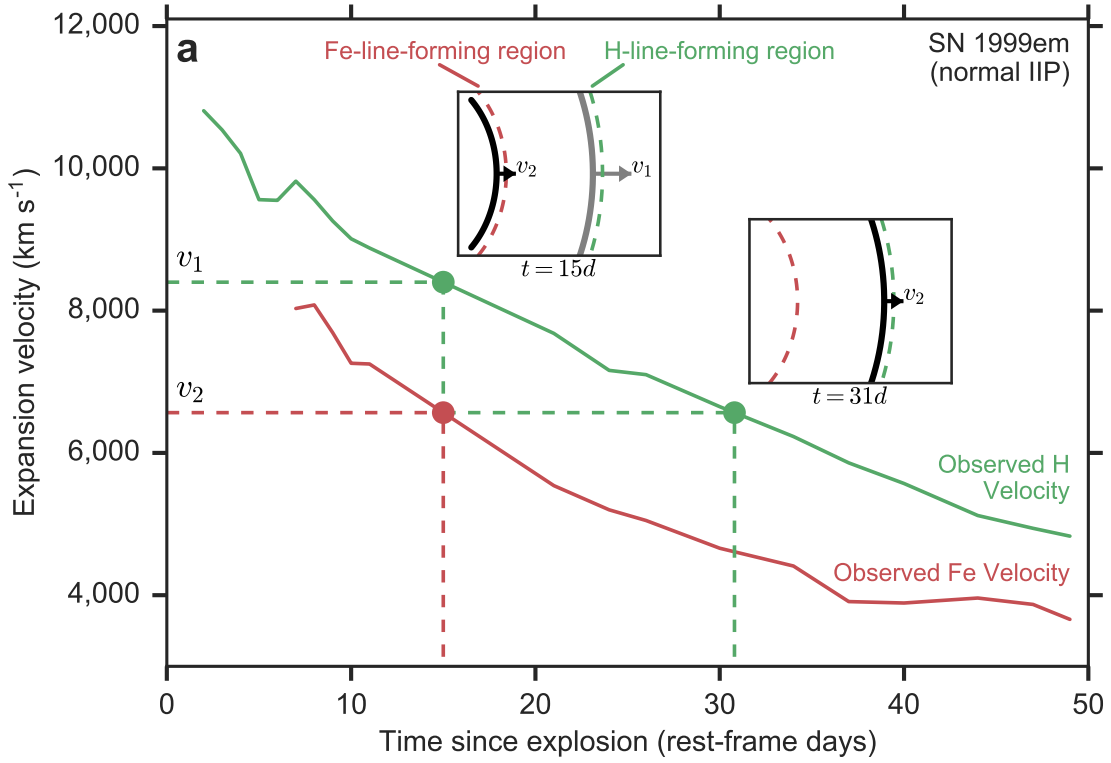


847

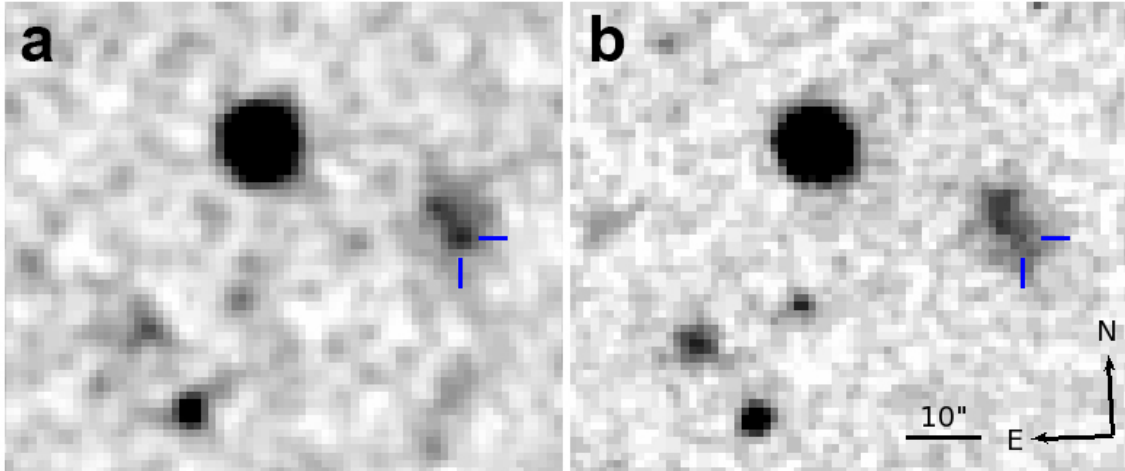
848 **Extended Data Figure 6** Spectra of iPTF14hls expressed in terms of normalized flux density  
 849 as a function of rest-frame wavelength taken on rest-frame days 207 (right before the rise to the  
 850 brightest peak in the light curve) and 232 (at the brightest peak in the light curve) after discovery  
 851 (solid lines). The similarity of the spectra indicate that the increase of  $\approx 50\%$  in luminosity observed  
 852 in the light curve between the two epochs is equal at all wavelengths. If the increase were only due



853 to the continuum flux, then the line emission on day 232 would have been diluted in the continuum  
854 (as simulated by the dashed line).



856 **Extended Data Figure 7** Evolution of the measured velocity gradient in the normal Type II-P  
857 SN 1999em<sup>22</sup> (**a**) and in iPTF14hls (**b**). At a given time, the H-line-forming region is at material  
858 expanding with velocity  $v_1$ , while the Fe-line-forming region is at material expanding with lower  
859 velocity  $v_2$  (top inset in panel **a**). For SN 1999em, the H-line-forming region soon reaches the  
860 material expanding at velocity  $v_2$  as it moves inward in mass (bottom inset in panel **a**) and  $v_2$  is  
861 measured in the H lines. For iPTF14hls, in contrast, the H-line-forming region does not reach  
862 the material expanding at  $v_2$  even after the time since discovery increases by a factor of 6. If the  
863 material were ejected at discovery, this would indicate an increase in the radius of the line-forming  
864 regions by a factor of  $\approx 6$ , which is unlikely given the observed velocity gradient between the H and  
865 Fe lines. If the material were ejected before discovery, on the other hand, the relative expansion  
866 in radius would be much smaller, thus offering one possible explanation for the constant velocity  
867 gradient observed in iPTF14hls.



868

869 **Extended Data Figure 8** Blue-filter images of the position of iPTF14hls (marked by blue ticks)  
870 from 1954 Feb. 23 (POSS; **a**) and 1993 Jan. 2 (POSS-II; **b**). A source is visible at the position of  
871 iPTF14hls in the 1954 image, which is not there in the 1993 image. Using aperture photometry, we  
872 find that the 1954 source is  $0.31 \pm 0.14$  mag brighter than the underlying host galaxy at that position,  
873 corresponding to a rough outburst magnitude of  $\approx -15.6$  at the luminosity distance of iPTF14hls,  
874 after removing host galaxy contribution and calibrating the field to the SDSS  $u+g$ -bands.

Line	Flux	Flux Error
[O II] 3727 Å	$2.050 \times 10^{-16}$	$1.152 \times 10^{-17}$
H $\beta$	$5.666 \times 10^{-17}$	$6.349 \times 10^{-18}$
[O III] 4958 Å	$1.742 \times 10^{-17}$	$6.130 \times 10^{-18}$
[O III] 5007 Å	$1.003 \times 10^{-16}$	$6.171 \times 10^{-18}$
H $\alpha$	$1.539 \times 10^{-16}$	$4.089 \times 10^{-18}$
[N II] 6583 Å	$1.361 \times 10^{-17}$	$4.095 \times 10^{-18}$

Table 1: iPTF14hls host-galaxy line fluxes (in  $\text{erg s}^{-1} \text{cm}^{-2} \text{\AA}^{-1}$ ). Errors denote  $1\sigma$  uncertainties.

Diagnostic	Metallicity	Lower Error	Upper Error
N06-N2 <sup>74</sup>	8.339	-0.126	+0.098
N06-R23 <sup>74</sup>	8.633	-0.166	+0.071
D02 <sup>75</sup>	8.334	-0.166	+0.139
PP04-N2Ha <sup>76</sup>	8.250	-0.059	+0.044
PP04-O3N2 <sup>76</sup>	8.309	-0.051	+0.037
M08-N2Ha <sup>77</sup>	8.458	-0.116	+0.076
M13-O3N2 <sup>78</sup>	8.252	-0.035	+0.025
M13-N2 <sup>78</sup>	8.249	-0.078	+0.060
KK04-N2Ha <sup>79</sup>	8.490	-0.127	+0.080
KD02comb <sup>80</sup>	8.386	-0.130	+0.055

Table 2: iPTF14hls host-galaxy  $12 + \log(\text{O}/\text{H})$  metallicity values under different diagnostics and calibrations. Error ranges denote  $1\sigma$  uncertainties.